

激光诱导荧光技术燃烧诊断的研究进展

朱家健*, 万明罡, 吴戈, 闫博, 田轶夫, 冯戎, 孙明波

国防科技大学空天科学学院高超声速冲压发动机技术重点实验室, 湖南 长沙 410073

摘要 激光诱导荧光(LIF)技术具有非扰动、实时原位测量、组分选择性强、灵敏度好、时空分辨率高等优点,可用于燃烧诊断中测量火焰的重要特征参数。介绍了 LIF 技术的原理及其在燃烧诊断中的应用,重点阐述了 LIF 技术在成像火焰瞬时结构、定量测量组分浓度、混合场温度、火焰温度和流场速度方面的研究进展,讨论了 LIF 技术在测量燃烧流场参数时的技术特点和挑战,展望了高速平面 LIF、体 LIF 和多场同步测量方面的发展趋势。

关键词 光谱学; 激光诱导荧光; 燃烧诊断; 发动机; 火焰结构; 温度; 流速

中图分类号 O436

文献标志码 A

doi: 10.3788/CJL202148.0401005

1 引言

燃烧为人类的生产和生活提供所需的能源,目前世界上超过 80% 的能源都是通过燃烧获得的^[1]。超燃冲压发动机^[2-3]、火箭发动机^[4-5]、燃气轮机^[6-7]、内燃机^[8]等都是通过燃料在发动机燃烧室内的燃烧获得维持发动机正常工作的推力。因此,深入研究燃烧机理,增强燃烧性能调控,有助于提高燃烧效率,降低燃烧污染物排放^[9],优化发动机的推力性能。

理论模型^[10-12]、数值计算^[13-14]和实验测量^[15-20]是研究发动机燃烧机理的三种关键手段。燃烧实验测量技术可为完善燃烧理论模型和改进数值计算方法提供可靠的校验,实验测量获得的火焰结构、组分浓度、当量比、火焰温度和流场速度等重要参数,有助于揭示发动机燃烧流场的特征和内在机制,为发动机燃烧室的设计和燃烧性能的优化奠定基础^[21]。

传统的实验测量方法为接触式物理探针法,如热电偶测温、热线风速仪测速。物理探针法直接将探测器侵入燃烧流场中,会造成流场、传热、催化、淬灭等干扰。火焰自发辐射成像(如高速摄影)为非接触式光学测量方法,能记录火焰结构及其动态演化过程且不会干扰燃烧流场,但自发辐射图像为路径

积分的结果,没有空间分辨率,且难以获得火焰的定量参数信息。

与物理探针法和自发图像成像法相比,激光诱导荧光(LIF)技术具有非扰动、实时原位测量、组分选择性强、灵敏度好、时空分辨率高等优点^[22]。在 LIF 测量时,将具有特定波长的激光导入燃烧流场中,待测组分吸收激光后向上能级跃迁,然后再向下能级跃迁时向外辐射出荧光,通过分析、处理和标定荧光信号,可获得火焰的瞬时结构、组分浓度、当量比、火焰温度和流速等信息。

自 Kychakoff 等^[23]用 LIF 成像火焰瞬时结构以来,LIF 技术被广泛应用于燃烧诊断中,且应用场合和测量参数还在不断拓展。应用场合从实验室基础层流和湍流火焰的诊断^[24-27]逐步发展到发动机燃烧室高温、高压和高速的复杂燃烧流场诊断^[28-31];测量参数从定性成像火焰瞬时结构和燃料分布^[32-34]发展到浓度^[35-36]、温度^[37-39]、流速^[40]等重要参数的定量测量,且逐步向高速^[41-42]、三维(3D)^[43-44]和多参数测量^[45-46]发展。

本文结合国防科技大学 LIF 技术燃烧诊断方面的研究工作,综述了 LIF 技术在燃烧诊断中的研究进展及其在发动机燃烧流场测量中的应用。首先介绍 LIF 技术的基础理论,然后论述了 LIF 技术在

收稿日期: 2020-07-01; 修回日期: 2020-07-28; 录用日期: 2020-09-15

基金项目: 国家自然科学基金(51606217, 91741205)、湖南创新型省份建设专项经费(2019RS2028)

* E-mail: jjzhu@nudt.edu.cn

测量火焰瞬时结构成像、组分浓度、当量比、火焰温度和流速等方面的研究进展,最后对 LIF 技术的发展趋势进行了展望。

2 平面激光诱导荧光基础理论

物质的电子能级、振动能级和转动能级等结构具有指纹识别作用,不同物质或同一物质在不同温度、速度和压力环境中的能级结构、粒子数分布均存在差异。燃烧化学反应产生的中间产物(如 CH、OH 和 CH₂O)具有特定的能级结构,这些组分吸收特定波长的激光光子能量后会被激发至高能级,位于高能级的粒子会返回低能级并发出具有光谱特征的 LIF 信号。LIF 能级跃迁示意图如图 1 所示,其中, v' 为振动能级。根据 LIF 信号的激发光谱、荧光光谱和荧光强度等信息可获得燃烧过程中的火焰瞬时结构、组分浓度、火焰温度等特征参数。

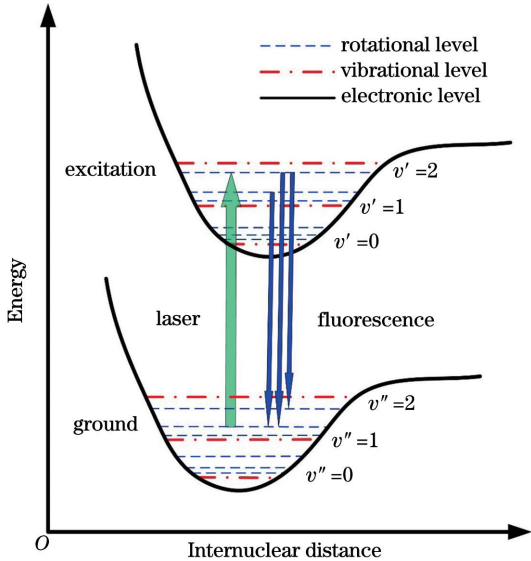


图 1 LIF 能级跃迁示意图

Fig. 1 Schematic diagram of the energy level transition of the LIF

根据单光子二能级结构模型^[47],得到 LIF 信号的强度 F 为

$$F = \frac{h\nu}{c} \frac{\Omega}{4\pi} \cdot l \cdot A \cdot N_1^0 \cdot \frac{B_{12}}{B_{21} + B_{12}} \frac{A_{21}}{1 + I_\nu^\nu / I_{\text{sat}}^\nu} \quad (1)$$

式中, $h\nu$ 为荧光光子的能量, h 为常量, ν 为频率, c 为真空中的光速, Ω 为信号接收立体角, A 为激光的聚焦面积, l 为激光沿光轴能观测到的长度, N_1^0 为激光激发前的下能级布居, B_{21} 和 B_{12} 分别为受激吸收和发射的爱因斯坦系数, A_{21} 为较高能级粒子的自发发射率, I_ν 为激光光谱强度, $I_{\text{sat}}^\nu =$

$c(A_{12} + Q_{21}) / (B_{21} + B_{12})$ 为饱和光谱强度,其中, Q_{21} 为淬灭速率。在弱激发状态,即 $I_\nu \ll I_{\text{sat}}^\nu$ 时,(1)式可表示为

$$F = \frac{h\nu}{c} \frac{\Omega}{4\pi} \cdot l \cdot A \cdot N_1^0 \cdot B_{12} \cdot I_\nu \cdot \frac{A_{21}}{A_{21} + Q_{21}} \quad (2)$$

在强激发状态达到饱和,即 $I_\nu \gg I_{\text{sat}}^\nu$ 时,(1)式可表示为

$$F = \frac{h\nu}{c} \frac{\Omega}{4\pi} \cdot l \cdot A \cdot N_1^0 \cdot A_{21} \cdot \frac{B_{12}}{B_{12} + B_{21}} \quad (3)$$

由(2)式和(3)式可知,通过测量荧光强度 F 能获得组分浓度 N_1^0 。但在弱激发状态,需要考虑淬灭速率 Q_{21} 对组分浓度定量测量的影响。在饱和状态,淬灭速率 Q_{21} 的影响可忽略。

双线 LIF 法通过测量上下能级的粒子数分布获得组分的温度信息,利用两束不同波长的激光激发同一物质的上下能级,收集两束激光激发后不同波长的荧光信号,再通过数据处理和标定等获得温度信息。双线 LIF 法测得的温度可表示为^[48]

$$T = \frac{-\Delta E/k}{\ln \frac{F_1}{F_2} + \ln \frac{I_2}{I_1} + 4 \ln \frac{\lambda_1}{\lambda_2} + \ln C} \quad (4)$$

式中, ΔE 为上下能级差, k 为玻尔兹曼常数, F_1 和 F_2 分别为两束荧光信号的强度, I_1 和 I_2 分别为两束激发激光的强度, λ_1 和 λ_2 分别为两束荧光信号的波长,常数 C 可通过标定已知温度的标准燃具获得。

为了将 LIF 技术应用于二维(2D)成像,通常利用光学透镜组将激光束制作成光片,形成平面 LIF (PLIF)。PLIF 光片的形成示意图如图 2 所示,其中,CL 为柱面凹透镜,SL 为球面凸透镜,激光片的厚度通常为 100 μm 量级。PLIF 可将测量范围拓

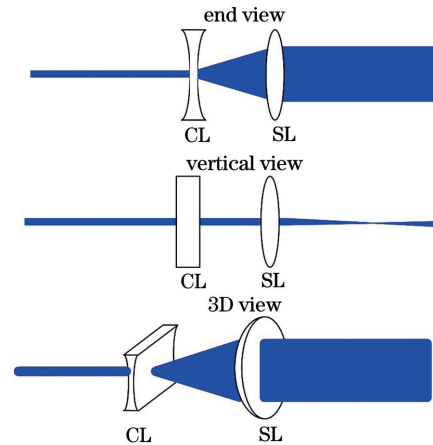


图 2 PLIF 光片的示意图

Fig. 2 Schematic diagram of the PLIF laser sheet

展至二维空间的特定平面,不受同一方向上不同截面自发辐射光信号空间积分效应的影响,且具有较高的空间分辨率。常用 PLIF 激光器的脉冲宽度约为 10 ns,相机的曝光时间可控制在几十纳秒量级,可以很好地滤除火焰的自发辐射光,且不受自发辐射时间上积分效应的影响。因此,PLIF 可以高时空分辨成像火焰结构、燃料分布和火焰温度。

3 PLIF 成像火焰瞬时结构

碳氢燃料燃烧过程中产生的重要中间产物(如甲醛 CH_2O 、次甲基 CH 、羟基 OH)可以作为火焰瞬时结构的标示物。 CH_2O 为火焰预热区的标示物, CH 为火焰反应区的标示物, OH 为火焰产物区的标示物。实际发动机中的燃烧都是湍流燃烧,存在燃烧化学反应与湍流流场的强耦合。在湍流作用下,火焰瞬时结构会发生扭曲、褶皱、破碎、局部熄火和重燃等变化,通过 PLIF 技术成像火焰瞬时结构有助于研究燃烧和湍流的相互作用机理。

3.1 单组分 PLIF

PLIF 通过高时空分辨成像 CH_2O 、 CH 、 OH 的二维分布,呈现火焰预热区、反应区和产物区的瞬时结构^[22]。表 1 为 CH_2O 、 CH 、 OH 与其他常用于燃烧诊断的荧光组分以及 PLIF 技术方案^[49-60]。

表 1 常见荧光组分及典型激发方案

Table 1 Common fluorescence species and typical excitation schemes

Species	Excitation wavelength /nm	Laser system	Detected fluorescence range /nm	Physical indication
OH	~282	dye laser ^[49] dye laser ^[50]	~309	product zone of hydrocarbon combustion
CH	~387	XeCl laser ^[51] Alexandrite laser ^[52]	~431	reaction zone of hydrocarbon combustion
CH_2O	~314	dye laser ^[53]	300-360	preheating zone of hydrocarbon combustion
	~355 ~352.48	Nd:YAG laser ^[54] dye laser ^[55]	380-550	
HCO	~259	Alexandrite laser ^[56]	280-350	heating releasing zone of hydrocarbon combustion
CN	~359	dye laser ^[57] Alexandrite laser ^[57]	~389	key intermediate species of nitrogen chemistry in combustion
NO	~226	dye laser ^[58]	~250	combustion emission
H-atom	~205	dye laser ^[59]	~656	two-photon process, key intermediate species in hydrocarbon combustion
O-atom	~226	dye laser ^[60]	~845	two-photon process, key intermediate species in combustion

图 3(a)为单组份 PLIF 实验系统示意图,主要由激光器、光路、探测器和时序同步控制器组成。图 3(b)~图 3(f)分别为开放式小型射流火焰 HCO 、 CH_2O 、 CH 、 OH 和 CH_3 单组分 PLIF 成像火焰瞬时结构的结果,可实现湍流火焰预热区、反应区、产物区和放热区的高时空分辨可视化^[56,61-63]。就 PLIF 成像火焰瞬时结构而言,主要包括改进常见组分(如 CH_2O 、 CH 、 OH)的激发方案、拓展测量的组分范围(如醛基 HCO 、氰基 CN 、 H 原子和 O 原子)以及开发光解-LIF(PF-LIF)技术。Carter 等^[64]提出了基于 CH 中 C-X 能级跃迁的荧光激发方案,可在提高 CH 荧光信号信噪比的同时降低所需激光脉冲的能量,从而利用现有激光器技术实现小型火焰 CH PLIF 的 10 kHz 频率测量,其中,激光单脉冲能量为 0.2 mJ。Zhou 等^[56]提出了适用于中低当量比预混火焰的 HCO PLIF 技术,实现了能表征燃烧释热率分布的 HCO 瞬时成像。Li 等^[63,65]提出了甲基 CH_3 的 PF-LIF 技术,利用波长约为 213 nm 的激光将 CH_3 光解为 CH ,然后基于 CH PLIF 技术对光解产生的 CH 进行成像;由于光解 CH_3 产生的 CH 浓度远远高于火焰原有的 CH 浓度,获得的荧光信号图像可视为 CH_3 的二维分布。

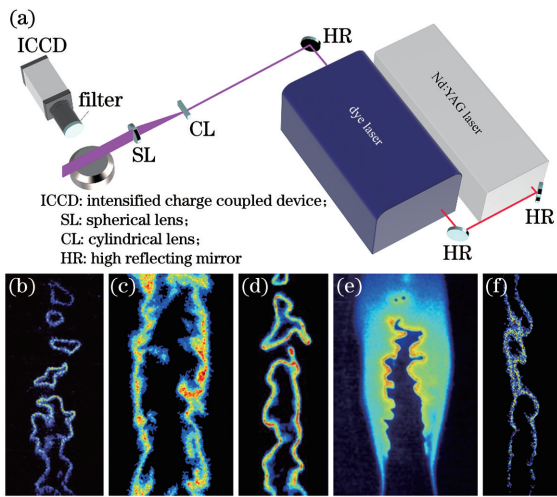


图 3 单组分 PLIF 成像的射流火焰。(a) 实验系统；(b) HCO PLIF^[56]；(c) CH₂O PLIF；(d) CH PLIF^[61]；(e) OH PLIF^[62]；(f) CH₃ PF-LIF^[63]

Fig. 3 Jet flame obtained by single-species PLIF imaging. (a) Experimental system; (b) HCO PLIF^[56]; (c) CH₂O PLIF; (d) CH PLIF^[61]; (e) OH PLIF^[62]; (f) CH₃ PF-LIF^[63]

与对开放空间火焰的成像不同, PLIF 成像发动机火焰瞬时结构是在封闭的燃烧室中进行的, 需要通过光学窗口引入激发激光, 并从光学窗口收集荧光信号。由于荧光信号较弱, 需要尽可能地降低壁面反射的激光, 限制了激发激光的脉冲能量。发动机的燃烧室需要在高速入口来流条件下, 在有限空间内组织燃料与空气的混合、燃烧, 燃烧室内反应强度高, 火焰背景辐射较强。此外, 还存在光学系统无法在线优化等难点。这些因素使 PLIF 成像发动机火焰结构时, 需要针对不同的测试工况和测试环境优化技术方案, 以提高荧光信号的信噪比。

目前, PLIF 成像发动机火焰结构大多采用 OH PLIF 技术^[30-31, 66-72], 原因是 OH 在火焰中的浓度相对较大, 其荧光效率高、荧光信号波长范围窄且处于紫外波段, 受火焰背景辐射干扰小。图 4(a)^[66] 与图 4(b)^[31] 为国防科技大学直连式超声速燃烧实验台上拍摄并采用 OH PLIF 成像凹腔区域火焰结构的图像。流向成像结果表明, 在凹腔内部、凹腔上方的剪切层都存在大量 OH 荧光信号, 证明了凹腔的高温回流稳焰机制是有效的; 成像结果显示, OH 大量分布于燃料横向射流反涡旋对的周围, 这表明射流引发的流场结构与燃烧室火焰结构存在密切联系。为了获得更精细的 OH 分布图像, Geipel 等^[69] 直接用一块焦距为 20 mm 的凸透镜作为相机镜头, 单幅图像的视场范围直径约为 6 mm; 通过步进电

机和导轨精确控制相机移动, 对燃烧室内不同位置的 OH 荧光信号进行高分辨率成像, 结果如图 4(c) 所示。Tian 等^[72] 利用 OH PLIF 对不同工况下超燃冲压发动机内的 OH 分布进行成像, 测量结果表明, 发动机内的燃烧具有较强的不稳定性。为了使发动机更适合光学诊断, 近年来用于光学诊断的发动机存在小型化、透明化的发展趋势^[71]。发动机小型化后, 相机得到的单幅图像可捕获更大的区域; 透明化后的发动机提供了便利的光学窗口, 为三维燃烧诊断技术^[73-74] 的应用创造了条件。

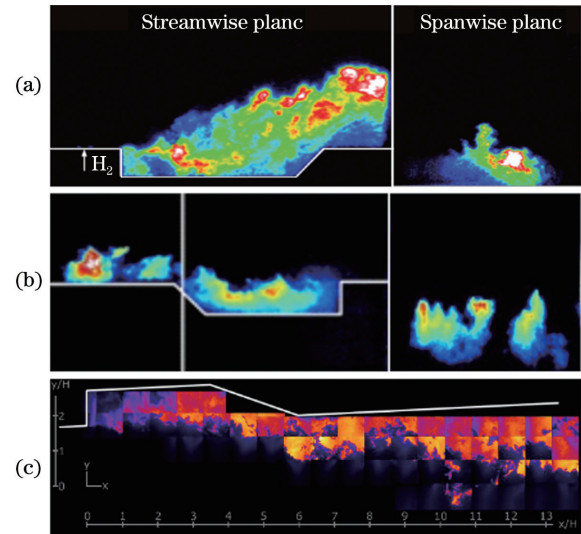


图 4 超燃冲压发动机瞬态火焰结构的 OH PLIF 成像。(a) 氢气喷注^[66]；(b) 乙烯喷注^[31]；(c) 乙烯喷注的高分辨率成像^[69]

Fig. 4 Instantaneous flame structure acquired by OH PLIF in scramjet engines. (a) Hydrogen injection^[66]; (b) ethylene injection^[31]; (c) ethylene injection with high-resolution imaging^[69]

尽管 CH PLIF 和 CH₂O PLIF 已广泛用于开放式小型火焰炉的燃烧研究^[18], 但其在发动机中的应用仍十分受限, 原因是燃烧室内的背景噪声较强, 导致荧光信号的信噪比偏低。Micka 等^[75-76] 利用 CH PLIF 对发动机燃烧进行研究时发现, 仅用窄带滤光片无法消除火焰的辐射背景光; 因此, 将一台相机放置在燃烧室的另一侧同时拍摄火焰辐射背景图像, 通过减背景提高 CH 图像的信噪比。基于 Alexandrite 激光器输出的二倍频 (波长约为 387 nm), 国防科技大学利用 CH PLIF 对凹腔火焰结构进行成像, 结果如图 5(a)^[77] 和图 5(b)^[31] 所示。可以发现, CH 荧光信号主要分布于凹腔剪切层附近, 这表明凹腔高温产物被卷入剪切层, 对剪切层火焰起到稳定作用, 如图 5(c) 所示。CH 反应层厚度

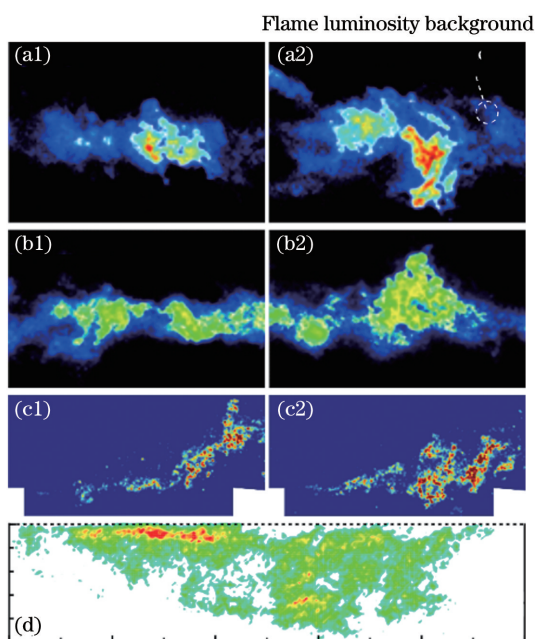


图 5 不同 PLIF 方法得到的瞬态火焰结构。(a)CH PLIF^[77];
(b)CH PLIF^[31]; (c)CH PLIF^[76]; (d)CH₂O PLIF^[78]
Fig. 5 Instantaneous flame structures obtained by
different PLIF methods. (a) CH PLIF^[77];
(b) CH PLIF^[31]; (c) CH PLIF^[76]; (d) CH₂O
PLIF^[78]

发生明显展宽并呈破碎状,符合湍流燃烧模式中破碎反应区的火焰特点。此外,还可以观察到部分区域内的荧光信号与火焰背景辐射强度相当。

利用 CH₂O PLIF 成像火焰结构时,激发激光的波长通常为 355 nm 左右,原因是该波长更便于通过三倍频 1024 nm 激光(由 Nd:YAG 激光器输出)获取,但 CH₂O 在该波长的荧光效率偏低,需要使用较大的激光能量以保证图像的信噪比,一般激光脉冲能量大于 100 mJ。成像发动机凹腔的流向截面时,入射激光能量越高,被凹腔底部金属壁面反射的激光能量也就越多,从而严重干扰荧光信号。为了解决该问题,Rasmussen 等^[78]将相机快门的触发延迟设置为 200 ns,实验中超燃冲压发动机燃烧室入口的来流温度为 430 K、总压为 512 kPa(低温、低压条件下 CH₂O 的荧光寿命较长,如果燃烧室总温、总压较高,CH₂O 荧光寿命会显著缩短,该方法不再适用),对 CH₂O 的成像结果如图 5(d)所示。Micka 等^[75-76]采用荧光效率更高的 352.48 nm 激发波长,降低所需的激光能量,但分析发动机的 CH₂O PLIF 数据时发现,激光片未覆盖的区域也可能出现类似于 CH₂O 荧光的背景信号,这表明图像数据的信噪比偏低。Allison 等^[79]利用 CH₂O PLIF 对发

动机燃烧室展向截面的火焰结构进行成像,激发激光由光学窗口入射到燃烧室,然后经对置的光学窗口离开,规避了金属壁面导致的激光反射问题。为了进一步提高荧光信号强度,还使用了窄频带激光激发技术,采用种子注入技术,将激光的中心波长调整至 355.818 nm,线宽降至约 120 MHz。Gabet 等^[80]的对比研究表明,采用 Nd:YAG 窄频带激光的三倍频激发 CH₂O 获得的荧光强度比宽频带激发增强了 2 倍。

3.2 多组分 PLIF

多组分 PLIF 指在极短时间内(火焰被认为处于冻结状态)对多种组分进行 PLIF 成像,选择的组分一般可标示火焰结构的不同区域,以获取更丰富、完整的火焰结构信息。为了避免不同组分入射激光、荧光信号间的相互影响,需借助时序控制器对不同组分的荧光激发与捕获时间进行精确控制。多组分 PLIF 成像火焰瞬时结构已被广泛用于开放式小型火焰炉的燃烧研究,如图 6 所示。图 6(b)为 Lu

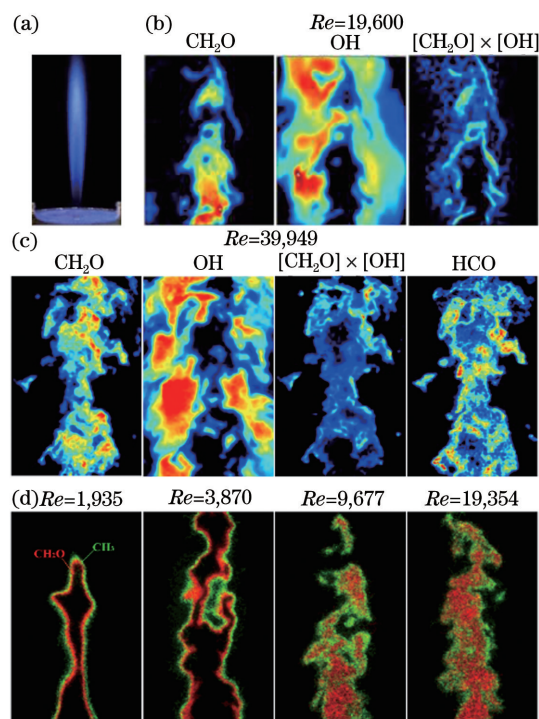


图 6 射流火焰的多组分 PLIF 成像。(a)射流火焰图像^[27];
(b)CH₂O/OH 同步 PLIF 图像^[27];
(c)CH₂O/OH/HCO 同步 PLIF 图像^[61];
(d)CH₃ PF-LIF 与 CH₂O PLIF 同步测量图像
Fig. 6 Multi-species PLIF imaging of the jet flames.
(a) Jet flame image^[27]; (b) simultaneous CH₂O/
OH PLIF image^[27]; (c) simultaneous CH₂O/OH/
HCO PLIF image^[61]; (d) simultaneous measurement
images of the CH₃ PF-LIF and CH₂O PLIF

等^[27]利用 $\text{CH}_2\text{O}/\text{OH}$ 同步 PLIF 对瞬态火焰结构成像的结果,火焰图像如图 6(a)所示,其中, Re 为雷诺数;图 6(c)为 Zhou 等^[61]的 $\text{CH}_2\text{O}/\text{OH}/\text{HCO}$ 同步测量结果;图 6(d)为国防科技大学用 CH_2O PLIF 与 CH_3 PF-LIF 同步成像的火焰结构。可以发现,标示火焰预热区的 CH_2O 组分最初仅分布在火焰锋面内侧,随着湍流强度的增加,火焰锋面逐渐扭曲、褶皱, CH_2O 最终分散在整个射流区域内,这表明燃烧模式最终进入分布式反应区,研究结果与 Zhou 等^[61]的结论相符。 CH_3 的展宽敏感性明显低于 CH_2O , 更靠近火焰释热锋面,具备在高湍流条件下用于成像火焰瞬时结构的潜力。

多组分 PLIF 的另一个重要应用是火焰释热率成像,火焰释热会明显改变局部温度和压力,进而影响流场状态,与许多重要的物理现象有关(如燃烧不稳定性^[66]),因此一直是燃烧研究的重点。 Paul 等^[81]提出利用 OH 和 CH_2O 荧光信号图像的乘积表征释热率分布,原因是 HCO 可作为释热率分布的标识物,而 HCO 的浓度与 OH 和 CH_2O 的浓度乘积成正比。对比 OH 和 CH_2O 的乘积图像与 HCO 荧光图像可知,两者的空间分布结构极其相似。目前关于多组分 PLIF 成像凹腔稳焰超燃冲压发动机燃烧室火焰瞬时结构的研究有 Micka 等^[75-76]的 $\text{CH}_2\text{O}/\text{OH}$ PLIF 工作,图 7(a)和 7(b)为凹腔稳焰超燃冲压发动机燃烧室展向截面和流向截面同步 $\text{CH}_2\text{O}/\text{OH}$ PLIF 图像。 $\text{CH}_2\text{O}/\text{OH}$ PLIF 同步测量结果揭示了发动机内的部分预混燃烧预热

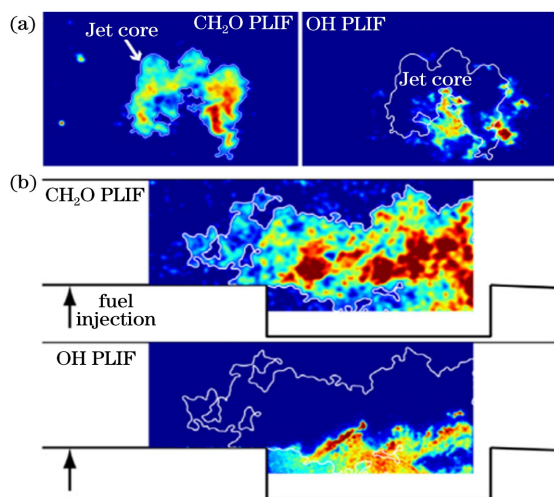


图 7 凹腔稳焰超燃冲压发动机燃烧室同步 PLIF 图像。

(a)展向截面;(b)流向截面^[76]

Fig. 7 Synchronous PLIF image of the cavity-stable flame scramjet combustion chamber. (a) spanwise plane;

(b) streamwise plane^[76]

区和已燃区的瞬时火焰结构,证明了该火焰结构受凹腔和横向射流引发的流场结构影响。

3.3 火焰结构参数的定量提取

利用 PLIF 成像火焰瞬时结构时,荧光信号不仅由激光能量、组分浓度决定,还受局部温度、压力及淬灭作用的影响。荧光信号反映了组分的空间分布结构,因此 PLIF 图像可用来定量提取火焰的结构参数。OH PLIF 图像的信噪比较高,不仅可用来提取火焰前锋面位置分布、曲率,还可用于估算火焰进度变量和火焰面密度^[69,82-83],如图 8(a)所示。 Wang 等^[82-84]基于 OH PLIF 图像定量分析了火焰

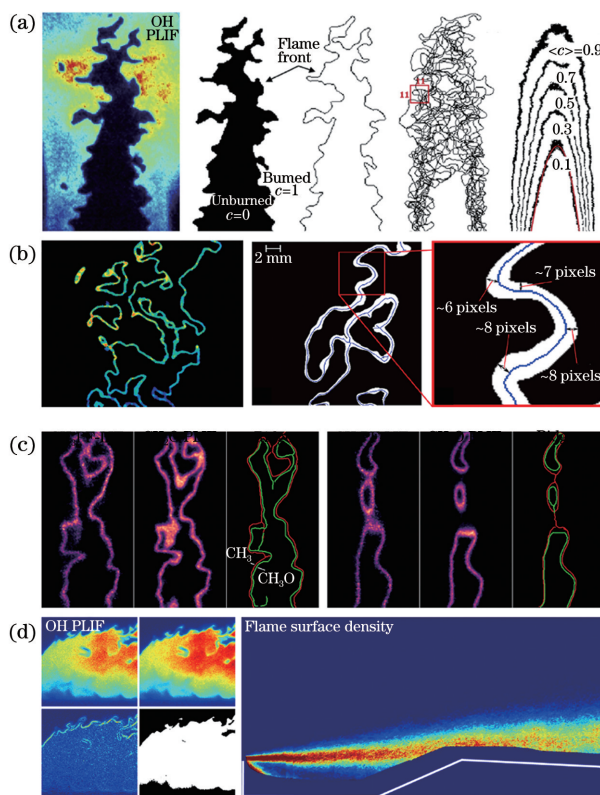


图 8 基于 PLIF 的火焰结构参数定量提取。(a) 基于 OH PLIF 的火焰面、火焰表面密度和进度变量定量提取^[83]; (b) 高湍流火焰的反应区厚度^[86]; (c) CH_3 PF-LIF/ CH_2O PLIF 同步测量图像和脊线提取结果; (d) 基于 OH PLIF 的超燃冲压发动机火焰面密度提取^[70]

Fig. 8 Quantitative extraction of flame structure parameters based on PLIF. (a) Quantitative extraction of flame surface, flame surface density and progress variables based on OH PLIF^[83]; (b) thickness of the reaction zone of the high turbulent flame^[86]; (c) CH_3 PF-LIF/ CH_2O PLIF simultaneous measurement image and ridge extraction results; (d) OH PLIF-based extraction of scramjet flame surface density^[70]

结构的特征参数,研究了富氢预混火焰的湍流火焰结构规律。Wu 等^[85]对比了基于 OH PLIF 和其他技术的本生灯火焰层流速度测量方案,发现基于 OH PLIF 的计算结果比实际值约低 5%。Skiba 等^[86]基于分水岭算法提取了 CH 反应层和释热层的厚度,以分析火焰结构随湍流的变化规律,拍摄的 CH PLIF 图像与 CH 组分厚度计算示意图如图 8(b)所示。针对 CH₂O PLIF/CH₃ PF-LIF 同步成像射流火焰结构图像,国防科技大学开展了定量火焰结构提取工作,获得了不同湍流度条件下,不同组分的曲率、厚度、密度、速度变量以及不同组分间距的变化规律。厚度计算结果表明,随着湍流强度的增加,CH₂O 的厚度有明显增加,CH₃ 的厚度则是缓慢增大。图 8(c)为 CH₃ PF-LIF/CH₂O PLIF 同步成像结果及其脊线提取图像。针对发动机的火焰结构定量提取,Geipel 等^[69-70]对发动机内火焰进行高分辨率 OH PLIF 成像,然后提取了燃烧室内火焰倾角、火焰曲率分布、火焰面密度等定量结构参数,结果如图 8(d)所示,并指出这些定量参数可用于超燃冲压发动机的仿真验证。

4 示踪 PLIF 成像组分浓度和温度

在发动机工作过程中,燃料和氧化剂的充分混合是高效燃烧的前提条件。而燃料与氧化剂混合的均匀性、组分浓度和温度分布特性会直接影响点火性能、火焰传播速度及火焰稳定性,进而影响发动机的性能和可靠性^[87-89]。燃烧为发动机的正常工作提供动力,燃烧效率直接决定发动机的推力性能。火

焰温度是研究发动机传热、热负荷及热防护等性能的基础,也是定量评估其燃烧状态、燃烧效率及其推力性能的重要参数^[90-92]。因此,对点火前混合场组分浓度、温度和燃烧过程的火焰温度进行定量测量有助于推动发动机燃烧机理的研究和发动机燃烧室的优化设计。

4.1 燃料分布、浓度和混合流场温度测量

在发动机工作过程中,燃料与氧化剂混合的均匀程度和温度分布特性表征对研究点火和燃烧具有重要意义。传统的燃气分析法在燃气接触取样后可实现燃气组分的定量分析,但这种接触式测量方法受复杂、恶劣发动机实验工况(高速、高湍流)限制,应用范围有限,因此,亟需发展高精度非扰动的激光光学诊断方法^[93-94]。

基于分子示踪的 PLIF 技术主要通过向混合燃气中加入示踪分子(如酮类、苯类、NO)直接获取混合燃气的空间分布信息,通过实验标定和后期数据处理进一步定量获取混合燃气的组分浓度、局部当量比、温度等信息^[89,94-95]。

对于分子示踪 PLIF 技术,常用的示踪粒子可分为有机分子(如甲苯、丙酮,3-戊酮)和无机分子(如 NO)两大类,常见的示踪分子特性参数如表 2 所示。美国斯坦福大学的 Lozano 等^[96-100]、德国杜伊斯堡-埃森大学的 Schulz 等^[101-104]、日本防卫大学的 Kashitani 等^[105]分别研究了不同示踪物质(如丙酮、3-戊酮、甲苯、萘、甲醛)的荧光光谱、寿命与环境温度、压强的关系,为示踪 PLIF 的应用和发展奠定了理论基础。

表 2 常见示踪物质的物理化学参数

Table 2 Physical and chemical parameters of common tracer substances

Parameter	Density / (g·cm ⁻³) 25 °C	Boiling point /°C	Autoignition temperature in air /°C	Excitation wavelength /nm	Fluorescence wavelength /nm	Measurement parameter	Application environment
Acetone ^[101]	0.79	56.1	465-727	225-325	300-500	component concentration/ temperature	low/high pressure, oxygen-free
3-pentanone ^[99,101]	0.81	102	425-608	248-312	300-500	component concentration/ temperature	low/high pressure, oxygen-free
Toluene ^[100]	0.87	110.6	480-810	~248	260-360	component concentration/ temperature	low pressure, oxygen-free
NO ^[95]	1.33×10 ⁻³	-151	-	~226	226-290	component concentration	low/high pressure, oxygen-free

研究示踪粒子物理特性和光学特性的同时,人们也将示踪 PLIF 技术应用于混合燃气组分浓度、温度等特性的研究,但受限于混合燃气组分浓度、温度的精确标定,实验主要研究分子示踪 PLIF 的定性表征,定量校准和测量研究工作较少,且目前主要借助示踪物质荧光的强度变化定性描述燃料的分布变化。文献[106-113]基于示踪 PLIF(如丙酮、甲苯、NO)进行了超燃冲压发动机、直喷式汽油发动机、全透明光学发动机等多类发动机燃气-空气混合分布显示实验,结果如图 9 所示。吉雍彬等^[114]利用丙酮 PLIF 技术获取了航空发动机扇段富油-贫油-淬熄(RQL)燃烧室冷态淬熄区燃气的分布结果。俞瑜^[115]用丙酮 PLIF 技术获取了低旋流部分预混燃烧器出口的燃气二维分布图像。孙明波等^[106-107]将丙酮 PLIF 技术用于超燃冲压发动机燃烧室的燃

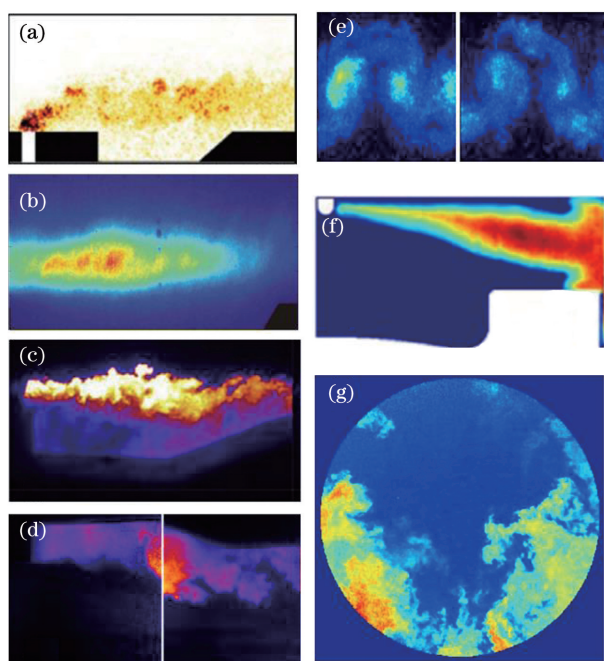


图 9 不同示踪 PLIF 在发动机燃料分布表征中的应用。(a) 丙酮 PLIF^[106-107]; (b) 煤油 PLIF^[108]; (c) NO PLIF^[109]; (d) NO PLIF^[110]; (e) 甲苯 PLIF^[111]; (f) 全透明光学单缸压燃机丙酮 PLIF^[112]; (g) 光学单缸机丙酮 PLIF^[113]

Fig. 9 Application of different tracer PLIF in the characterization of engine fuel distribution. (a) Acetone PLIF^[106-107]; (b) kerosene PLIF^[108]; (c) NO PLIF^[109]; (d) NO PLIF^[110]; (e) toluene PLIF^[111]; (f) fully transparent optical single-cylinder compressor acetone PLIF^[112]; (g) optical single-cylinder acetone PLIF^[113]

气混合特性(来流 Mach1.7)研究,获取的丙酮 PLIF 图像与大涡模拟结果基本一致。

在基于示踪 PLIF 技术的混合燃气组分、温度定量测量方面,丙酮、3-戊酮等酮类示踪物质具有毒性小、高饱和蒸气压、压力响应小等优点,被广泛应用于发动机局部当量比、混合燃气浓度、温度等参数的测量^[101];甲苯具有吸收截面大、量子产率高等优点,在发动机测量方面具有较大的应用前景,但该物质易受氧淬灭、压力影响,仅适用于常压无氧环境测量^[100];NO 能反映低温非反应区域的温度场信息,但不适用于燃料分布区域测量(容易和燃料进行反应),且毒性较大^[116-117]。在混合燃气组分定量测量方面,文献[35]、文献[118-121]开展了发动机混合燃气当量比的定量测量实验,结果如图 10 所示。赵纬等^[122-124]也进行了相关研究,Lind 等^[120]基于丙酮 PLIF 技术的 DISI 发动机浓度测量不确定度约为 4.5%。赵纬^[122]利用丙酮 PLIF 和标准定容器(可变压力)标定的形式对天然气发动机喷射射流流场燃气组分浓度分布进行了定量测量。马骁等^[123-124]利用示踪 PLIF 技术(示踪粒子为三乙胺和苯)测量了缸内直喷汽油机内混合气体的浓度分布,获得了燃油轻、中、重三种不同工况下缸内混合气体的浓度分布图像。此外,混合燃气测量结果的标定和校准是示踪 PLIF 技术的关键,目前大多数定量测量结果是通过标准定容器标定和质谱测量标定的方法进行校准,但这两种方法在发动机湍流场(压力、组分分布不均)测量中校准难度较大,因此如何利用高精度的组分定量测量技术进行精准标定仍然是这类示踪技术的难点和热点。

在温度测量方面,由于温度敏感性、饱和蒸气压等原因,通常使用丙酮、戊酮和甲苯等示踪 PLIF 技术。文献[125-129]基于单线/双线示踪 PLIF 技术开展了发动机混合燃气温度测量实验研究,结果如图 11 所示。Rothamer 等^[99]基于双线 3-戊酮 PLIF 测温技术使内燃机(IC)的温度测量精度达到 2.1%,Willman 等^[128]利用激光诱导光栅光谱单点测温技术(测温精度小于 1%)对单线双示踪物质 PLIF 技术(甲苯和异辛烷)进行校准,获得了 DISI 单缸光学引擎内燃气温度场结果,如图 11(d)所示。张万里等^[130]建立了单线双示踪 PLIF 系统(激发激光的波长为 266 nm,示踪剂为三乙胺和三戊酮),获得了不同示踪剂的荧光强度及其比值随温度、压强和浓度的变化关系,并将标定结果用于发动机缸内混合气体的温度和浓度测量。

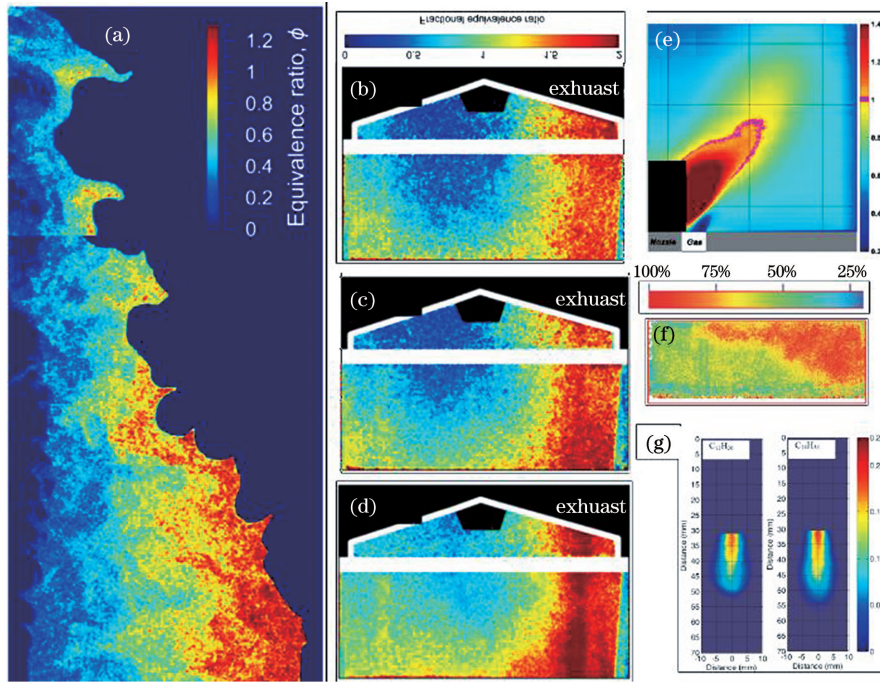


图 10 不同示踪 PLIF 在发动机混合燃气组分测量上的应用。(a)V 形火焰 3-戊酮 PLIF^[35]; (b)汽油发动机丙酮 PLIF^[118]; (c)汽油发动机甲苯 PLIF^[118]; (d)汽油发动机 TMB PLIF^[118]; (e)单喷射航空燃气轮机甲苯 PLIF^[119]; (f)IC TEA/丙酮 PLIF^[120]; (g)高压燃气喷雾室正十二烷/正十六烷 PLIF^[121]

Fig. 10 Application of tracer-PLIF to measure the equivalence ratio and fuel distribution in the different engines. (a) 3-pentanone PLIF in a V-shaped flame^[35]; (b) acetone PLIF in a gasoline engine^[118]; (c) toluene PLIF in a gasoline engine^[118]; (d) TMB PLIF in a gasoline engine^[118]; (e) toluene PLIF in a single-injector burner^[119]; (f) TEA/acetone PLIF in an IC engine^[120]; (g) n-dodecane/n-hexadecane PLIF in a high pressure chamber^[121]

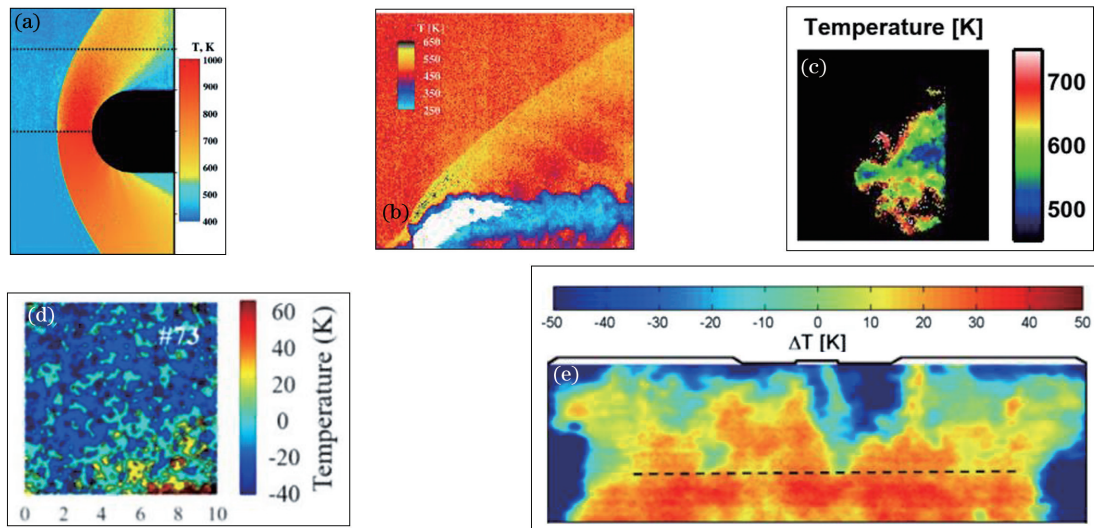


图 11 不同示踪 PLIF 在发动机混合燃气温度测量中的应用。(a)膨胀管甲苯-PLIF 测温^[125]; (b)超声速膨胀管甲苯-PLIF 测温^[126]; (c)HCCI 发动机丙酮/3-戊酮 PLIF 测温^[127]; (d)DISI 单缸光学发动机甲苯/异辛烷双示踪 PLIF 测温^[128]; (e)HCCI 发动机甲苯 PLIF 测温^[129]

Fig. 11 Application of tracer-PLIF in measuring the temperature distribution of different engines. (a) Temperature distribution of the expansion tube using toluene PLIF^[125]; (b) temperature distribution of the supersonic expansion tube using toluene PLIF^[126]; (c) temperature distribution of HCCI engine using acetone/3-pentanone PLIF^[127]; (d) temperature distribution of the DISI single-cylinder optical engine using toluene/isooctane PLIF^[128]; (e) temperature distribution of HCCI engine using toluene PLIF^[129]

4.2 燃烧场火焰温度场测量

发动机内湍流燃烧环境极其复杂,具有高速、高压和高温等特点,且发动机燃烧产生的积碳对激光诊断技术的影响较大(积碳散射、吸收、自发辐射等)^[90-91,131-132],导致大多可用于气体燃烧环境中的激光二维测温技术(如滤波瑞利散射测温技术^[133]、双线 OH PLIF 测温技术^[134])难以适用。目前获取发动机内部温度及热流场信息的方式仍以数值仿真为主,缺乏实时、准确的二维温度测量手段。

双线原子 LIF(TLAF)技术是一种可适用于积碳多、高温、高湍流燃烧环境的二维温度场测量技术。通过在燃料中添加特殊示踪原子(如 In, Ga 和 Th),再采用不同波长的激光激发示踪原子从低能级跃迁到高激发态,高激发态原子向较低能级跃迁产生荧光,根据不同波长荧光的强度分布比值可直接获取燃烧火焰温度场分布^[37,39,135-136],如图 12 所示。该技术具有温度敏感性较好、淬灭效应影响低、时空分辨率高及测温范围宽等优点。

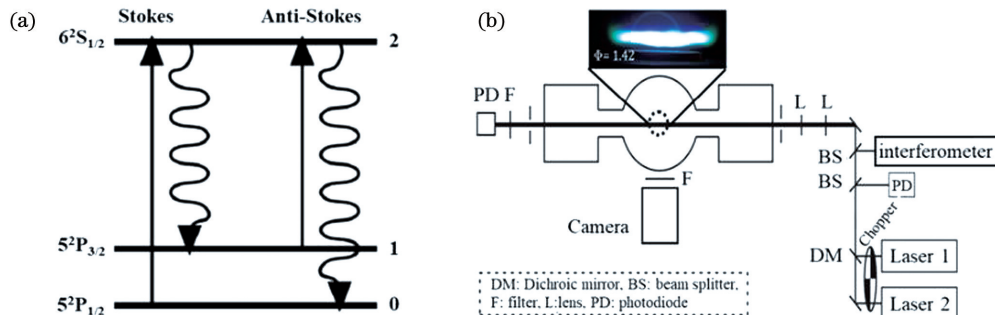


图 12 TLAF 技术示意图。(a) In 原子三能级示意图^[37]; (b) TLAF 测量系统示意图^[39]

Fig. 12 Schematic diagram of the TLAF technique. (a) Three-level diagram of the In atom^[37]; (b) schematic diagram of the TLAF measurement system^[39]

示踪原子的种类、注入、分散是 TLAF 技术研究的重点,目前报道的示踪原子种类主要包括 In、Ga 和 Th 等^[37,39,48],如图 13 和表 3 所示,其中,P 为原子能级。Th 原子有剧毒,在 3000 K 温度以下敏感性较低;Ga 原子在 1000 K 温度以下荧光强度随着温度变化的曲率较大,但在 1000 K 温度以上变化曲率较小,可用于低温(小于 1000 K)的流场测量;In 原子具有温度敏感性较高(500~2800 K)、可见波段激发等特点,因此常用来测量火焰温度^[48]。

表 3 TLAF 技术中不同示踪原子相关物理常数^[48]

Table 3 Relevant physical constants for the different atoms used for TLAF^[48]

Atomic element	Energy gap /cm ⁻¹	Transitions	Fluorescence wavelength /nm
Ga	826.19	4P _{1/2} → 5S _{1/2}	403
		4P _{3/2} → 5S _{1/2}	417
In	2212.598	5P _{1/2} → 6S _{1/2}	410
		5P _{3/2} → 6S _{1/2}	451
Th	7792.7	6P _{1/2} → 7S _{1/2}	378
		6P _{3/2} → 7S _{1/2}	535

目前,基于 In 原子的 TLAF 技术多采用注入 InCl₃ 的方法引入 In 原子,由于 InCl₃ 需经过火焰面才能分解产生 In,因此,仅能探测高温火焰面后

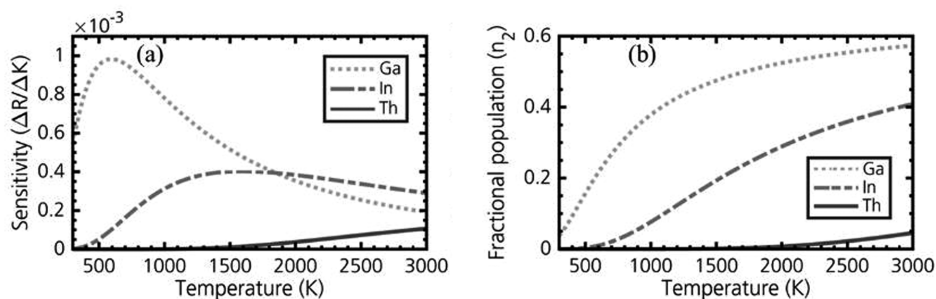


图 13 典型示踪原子的温度特性。(a) TLAF 中不同示踪原子的温度敏感性; (b) 示踪原子的上能级粒子数分布随温度的变化情况^[48]

Fig. 13 Temperature characteristics of typical atomic elements. (a) Temperature sensitivity of the atomic elements for TLAF; (b) variation of the particle number distribution of the upper energy level of the tracer atom with temperature^[48]

的温度分布;同时 InCl_3 溶液不易挥发,导致荧光测量图像信噪比低^[39,48,137]。Chan 等^[138-139]采用激光烧蚀 In 金属的方法注入 In 原子,可增加示踪原子的空间测量范围,同时可通过调制激光频率和功率

的方式提高注入 In 原子的浓度。Münsterjohann 等^[140-141]采用喷雾热解氧化铟和 TMI 的方式提高注入 In 原子的数量,如图 14 所示,这几种方法均被证实可明显提高 TLAF 图像的信噪比。

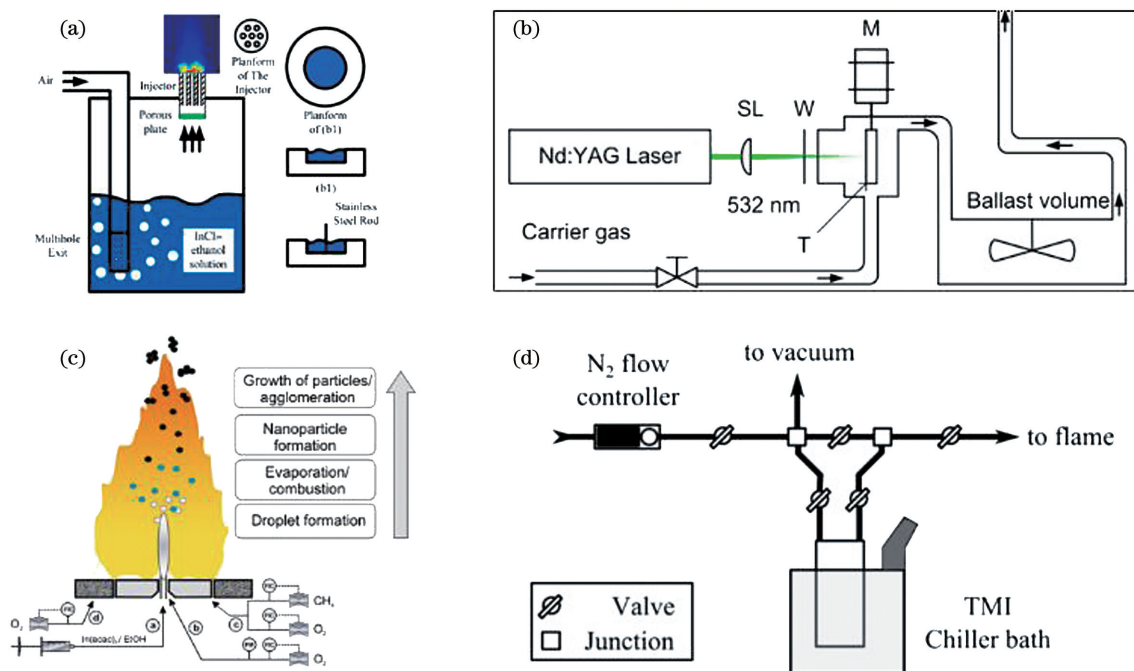


图 14 不同 In 原子示踪注入方法。(a) InCl_3 溶液注入^[137]; (b) 激光烧蚀 In 金属注入^[139]; (c) 喷雾热解 In_2O_3 注入^[140]; (d) 喷雾热解 TMI 注入^[141]

Fig. 14 Different seeding methods for the In atom. (a) InCl_3 solution seeding^[137]; (b) In seeding by laser ablation^[139]; (c) In_2O_3 seeding by flame spay pyrolysis^[140]; (d) TMI seeding by spray pyrolysis^[141]

TLAF 技术目前主要用于实验室研究阶段,包括线性和非线性 TLAF 技术的研究。针对线性 TLAF 技术,人们主要利用连续激光器和高频光电倍增管开展单点温度测量技术的研究^[142-143],采样频率可达到 10 kHz 以上^[142],测量精度可达到 8 K 左右^[143]。随着高能脉冲激光器和高量子效率 CCD 相机的发展,线性 TLAF 技术逐渐在二维温度场测量方面崭露头角,文献^[37, 39, 140, 144]利用层流和射流火焰开展了二维温度场测量实验研究,结果如图 15 所示。由于激光能量和示踪粒子浓度较低,In 原子荧光探测强度较弱,温度测量结果多为多张荧光图像累加,时间分辨率较低,不适用于湍流燃烧场瞬态测量分析。

为了进一步提高 TLAF 测量信号的信噪比,需要增加注入示踪原子的浓度或提高激光功率。Medwell 等^[145]提出并通过实验验证了非线性 TLAF (NTLAF) 是一种很有前景的湍流燃烧场二维温度测量技术,如图 16(a) 所示。Chan 等^[146]将 NTLAF 应用于含有碳烟的燃烧火焰测量,证明了

NTLAF 技术具有较强的抗碳烟干扰能力,并发现 NTLAF 荧光信号的主要干扰来源于积碳的先行物多环芳烃 (PAH)。Gu 等^[147]利用带宽为 1.2 nm 的窄带滤光片有效滤除了 PAH 对荧光信号的干扰,提高了测温精度。文献^[147-149]将 NTLAF 技术应用到层流、扩散燃烧火焰中进行了温度测量实验,结果如图 16(b)~图 16(e) 所示,同时采用热电偶或 CARS 技术对温度测量结果进行了校准。其中, Foo 等^[149]获得的瞬态荧光测量图像信噪比可以达到 4.8 以上,温度测量不确定度为 ± 139 K。Sun 等^[150]将基于激光模式和能量波动修正算法引入 NTLAF 技术进一步提高了 NTLAF 的测温精度,并基于湍流煤烟火焰开展了温度场测量实验研究,结果如图 16(b) 所示,结果表明,NTLAF 技术的相对测量不确定度可以达到 4.1% (200 幅图像的累加),空间分辨率达到 $550 \mu\text{m} \times 550 \mu\text{m}$ 。这些关键技术的研究极大推进了 NTLAF 的发展,但 NTLAF 测温校准过程比较复杂,不仅需要温度测量结果进行标定,还需对 NTLAF 测量中的多个

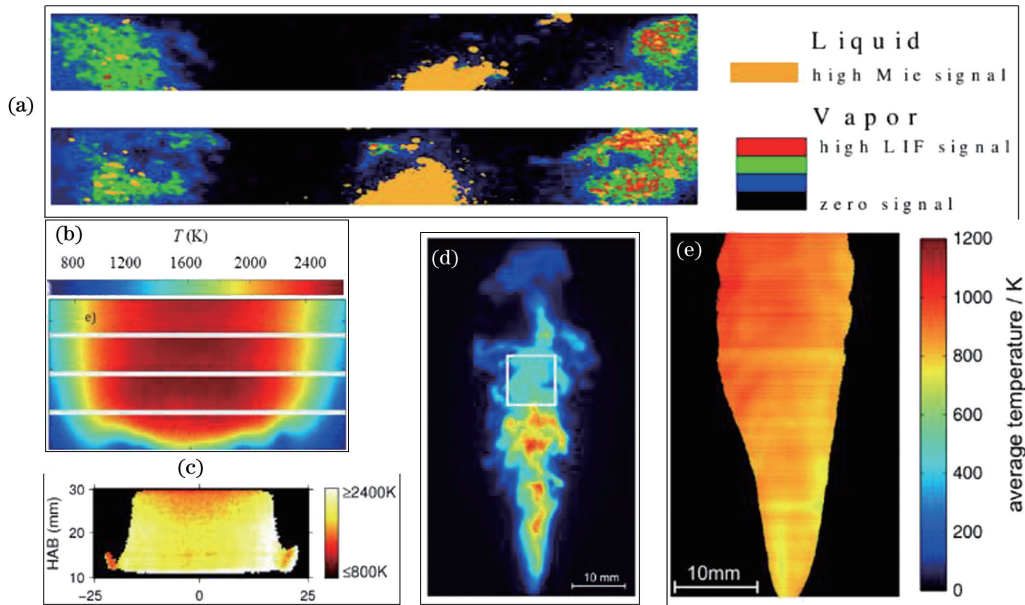


图 15 In 原子示踪线性 TLAF 测量的燃烧场温度分布。(a) TLAF 和米散射图像^[144]；(b)^[39]~(c)^[37]层流预混火焰的平均温度场分布；(d) 甲烷/空气射流预混火焰的荧光瞬态分布图像^[140]；(e) 甲烷/空气射流预混火焰的平均温度场^[140]

Fig. 15 Combustion field temperature distribution measured by linear TLAF with In atoms as tracers. (a) TLAF and Mie scattering image^[144]；(b)^[39] - (c)^[37] average temperature field distribution of laminar premixed flame；(d) fluorescence transient distribution image of methane/air jet premixed flames^[140]；(e) average temperature field of methane/air jet premixed flame^[140]

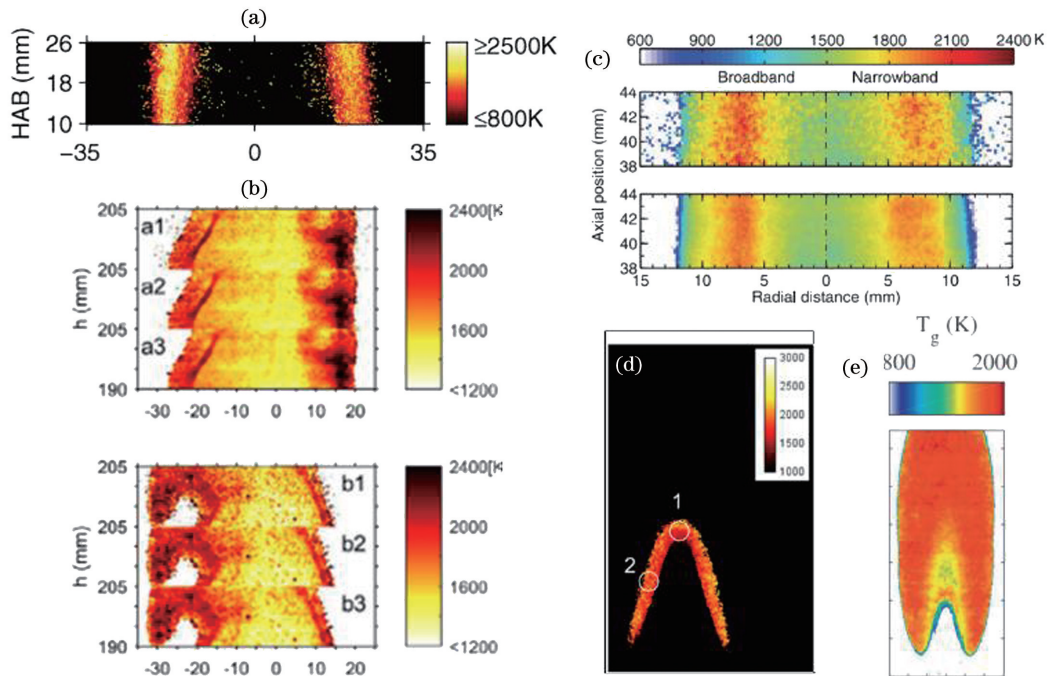


图 16 In 原子示踪非线性 TLAF 测量的燃烧场温度。(a) 层流预混火焰温度分布^[145]；(b) 非预混火焰温度分布^[150]；(c) 非预混火焰温度分布^[147]；(d) 槽式燃烧器温度分布^[148]；(e) 非预混火焰温度分布^[149]

Fig. 16 Combustion field temperature distribution measured by nonlinear TLAF with In atoms as tracers. (a) Temperature distribution in a laminar premixed flame^[145]；(b) temperature distribution in a non-premixed flame^[150]；(c) temperature distribution in a non-premixed flame^[147]；(d) temperature distribution in a slot burner^[148]；(e) temperature distribution in a non-premixed flame^[149]

系数进行标定,因此如何利用高精度测量技术同步精确地对测量参数进行标定是这类技术实现发动机燃烧火焰温度场测量的关键^[151]。Fang 等^[152]提出了一种基于单参数模型和可调谐二极管激光吸收光谱(TDLAS)技术的校准方法,只需一个系统参数和 TDLAS 技术获取的平均温度信息就可以实现 NTLAF 多参数标定,实验测量温度场的不确定度为 4.5%,与 TDLAS 和瑞利散射测温结果的偏差均小于 50 K。

综上所述,分子示踪 PLIF 技术为发动机燃烧流场的实验研究提供了新手段,其测量优势在于混合场浓度和温度、火焰温度等重要参数的高时空分辨瞬态测量,但还需解决示踪分子均匀注入、测量参数精确校准等问题。TLAF 技术作为一种新型的燃烧场温度诊断方法,在含有碳烟的燃烧场温度测量中具有很大的优势,有望用于复杂恶劣的发动机实验工况条件。但实现示踪原子的均匀注入、弱荧光信号的高效探测和温度参数的精确标定仍是这类技术应用到发动机测量中的关键问题。

5 基于 PLIF 技术测量燃烧流场速度分布

速度是燃烧流场的重要参数之一,对分析燃烧流场特性、支撑实际燃烧装置的设计能发挥关键作用。分子标记测速(MTV)^[40]技术作为速度测量的前沿技术,具有散播方式简单、随流性好等优势,在高速流场和燃烧场中得到了广泛的应用。

传统的 MTV 技术通常用激光束分别对示踪分

子进行写入和读取,进而实现速度测量,如图 17 所示。其中, t_0 为初始时刻。写入过程指激光与流场中特定分子相互作用,改变其状态或生成新的分子(如图中的符号 T),这一过程标记示踪分子的初始位置。读取过程是对示踪分子的显示过程,通常利用 PLIF 技术或直接拍摄示踪分子辐射光实现。标记分子的浓度会随时间衰减,其寿命(荧光寿命)需要大于写入和读取的时间间隔 Δt ,是决定测速技术应用范围的重要指标,可利用标记分子的位移 d 和时间间隔 Δt 获得速度信息。

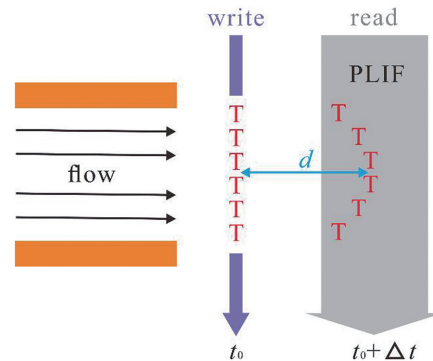


图 17 MTV 测速技术原理图

Fig. 17 Schematic diagram of the MTV technology

PLIF 测速技术是指以 PLIF 技术作为显示手段获得速度信息的一类测速方法,是 MTV 技术的关键组成部分。常用的示踪分子包括 OH、O₃、NO、Kr 和 NH 等,表 4 为近年来人们研究的 PLIF 测速技术及使用的示踪分子等参数,其中, λ_{write} 、 λ_{read} 分别为写入波长、读取波长, M 为任意分子,通常称为第三体。

表 4 PLIF 测速技术的参数

Table 4 Parameters of the PLIF speed measurement technology

Velocimetry	Tracer	λ_{write}/nm	Excitation	λ_{read}/nm
APART	NO	193 ^[153] /355 ^[154]	$N_2 + h\nu_{193\text{ nm}} \rightarrow N_2^+ + e^-$ $N + O_2 \rightarrow NO + O$	226
VENOM	NO	193 ^[155] /308 ^[156] /355 ^[157]	$NO_2 + h\nu_{355\text{ nm}} \rightarrow NO + O$	226
KTV	Kr	214.7 ^[158]	$Kr + 2h\nu_{214.7\text{ nm}} \rightarrow Kr^*$	760.2 ^[158] /769.5 ^[159]
HTV	OH	193 ^[40]	$H_2O + h\nu_{193\text{ nm}} \rightarrow OH + H$	248 ^[160] /283 ^[40] /308 ^[161]
OTV	O ₃	193 ^[160]	$O_2 + h\nu_{193\text{ nm}} \rightarrow O + O$ $O + O_2 + M \rightarrow O_3 + M$	248
NH-PLIF	NH	355 ^[162]	$N_2 + 6h\nu_{355\text{ nm}} \rightarrow N_2^+ + e^-$ $N + H_2O \rightarrow NH + OH$	337

5.1 基于 NO PLIF 的 APART/ VENOM 测速

以 NO 作为示踪分子的 PLIF 测速技术已经得到广泛应用,但产生 NO 的方式有很多种。空气光

解重组示踪测速(APART)技术通过光解空气产生 NO,不需要散布其他示踪分子。Dam 等^[163]在低速层流条件下,测得气流的速度为(1.11 ± 0.05) m/s。

Laan 等^[164] 在 3 马赫高速自由来流条件下用 APART 技术获得气流的速度为 (630.8 ± 2.7) m/s, 单幅测速精度可达 2%。Bearden 等^[154] 提出用波长为 355 nm 的固体激光代替波长为 193 nm 的 ArF 准分子激光, 实验得到的 NO 浓度和 PLIF 图像信噪比较低。APART 技术需要较高的激光能量密度, 且对流场的要求较高。

Orlemann 等^[156] 提出的振动激发 NO 测速 (VENOM) 技术利用激光光解 NO₂ 产生 NO, 在低压常温条件下, 当空气中 NO₂ 散布浓度达 600×10^{-6} 时, 测得 NO 的寿命可达 20 ms。Bathel 等^[157, 165-166] 在美国航空航天局 (NASA) 兰利研究中心的风洞中 ($Ma = 10$) 实现了单幅高超声速边界层转换的速度测量, 结果如图 18(a) 和图 18(b) 所示, 同时修改了 PLIF 系统和风洞模型^[166], 有效提高了图像的信噪比并减少了实验不确定性 (约 2 倍), 单幅图像的速度测量不确定度为 44 m/s。基于双线 LIF 测温^[167] 原理, Sánchez-González 等^[168] 实现气流的速度和温度测量。ElBaz 等^[155] 提出由激光光解 N₂O 产生激发态的 NO, 测速结果如图 18(c) 和图 18(d) 所示, N₂O 无毒无腐蚀性, 相比 NO₂ 更适合开放环境下的测量。直接激发流场中的 NO 也是一

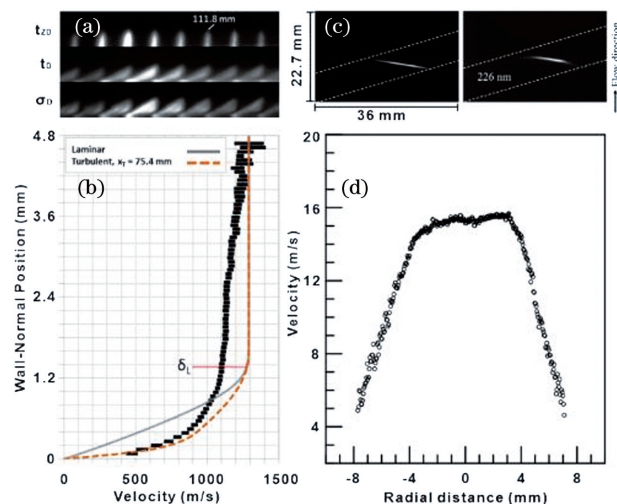


图 18 典型测速剖面图像。(a) 超声速边界层流动 NO PLIF 图像^[157]; (b) 超声速边界层流动速度分布^[157]; (c) 低速射流 NO PLIF 图像^[155]; (d) 低速射流速度分布^[155]

Fig. 18 Typical profile of velocimetry images. (a) NO PLIF images in a supersonic boundary layer^[157]; (b) velocity distribution in a supersonic boundary layer^[157]; (c) NO PLIF images in a low speed jet flow^[155]; (d) velocity distribution in a low speed jet flow^[155]

种可行的标记方法^[169], 但激发态的 NO 易受到 O₂ 等分子碰撞淬灭, 使荧光寿命更短, 只适用于超高速流场。Dai 等^[170] 在中国空气动力研究与发展中心的高超声速风洞 (6~12 马赫) 中开展基于 NO PLIF 的速度测量, 平均自由流速度为 3.32 km/s, 不确定度为 5.8%。

NO PLIF 测速技术在测速过程中利用的 NO_x 属于有毒气体, 因此不适用于开放流场尤其是大尺度流场; 且在高温或反应流中 NO_x 和 N₂O 易发生解离或参与化学反应, 导致 PLIF 信噪比降低, 因此这类技术大多应用在常温或低温状态下的非反应流场。

5.2 基于 Kr PLIF 的 KTV 测速

Parziale 等^[158, 171] 提出的 Kr 分子示踪测速 (KTV) 技术是一种利用 Kr 作为示踪分子的 PLIF 测速技术, 近年来被广泛应用于高速流场测量。KTV 技术的原理是利用波长为 214.7 nm 的激光激发产生亚稳态 Kr, 标记流场初始位置; 一定延迟时间后, 通过 PLIF 技术显示 Kr 的最后位置。在碰撞严重的流场环境下, 亚稳态 Kr 的尺寸为 10 μs 量级。Parziale 等^[158] 在非完全膨胀射流中对 KTV 技术的测速能力进行研究, 图 19 为 KTV 测速装置和

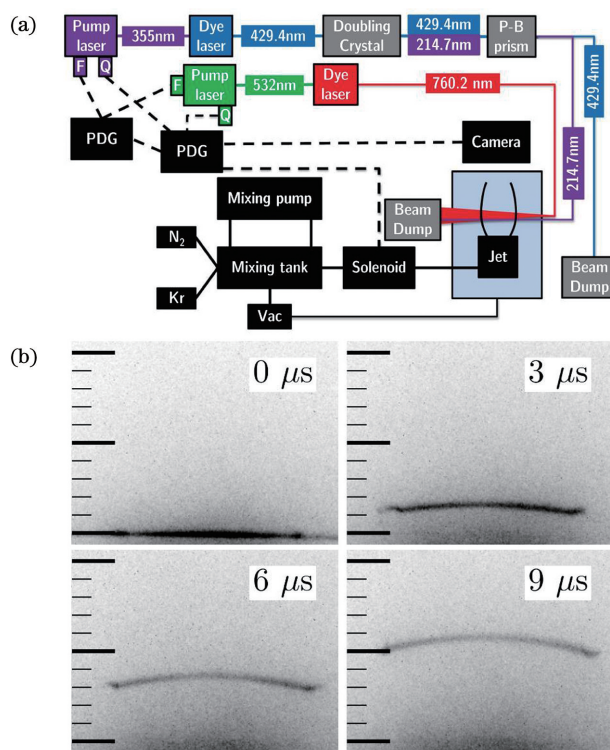


图 19 KTV 技术。(a) KTV 测速装置的示意图; (b) 典型的测速结果^[158]

Fig. 19 KTV technique. (a) Schematic of the KTV speed measurement device; (b) Typical speed measurement results^[158]

典型测速图像, 测量结果表明, 射流出口速度为 707 m/s。

基于 KTV 技术分别在超声速风洞 ($Ma = 2.7$)^[172] 和高超声速风洞 ($Ma = 10, Ma = 14$)^[159] 实现自由来流的速度测量, 结果如图 20(a) 所示^[159]。

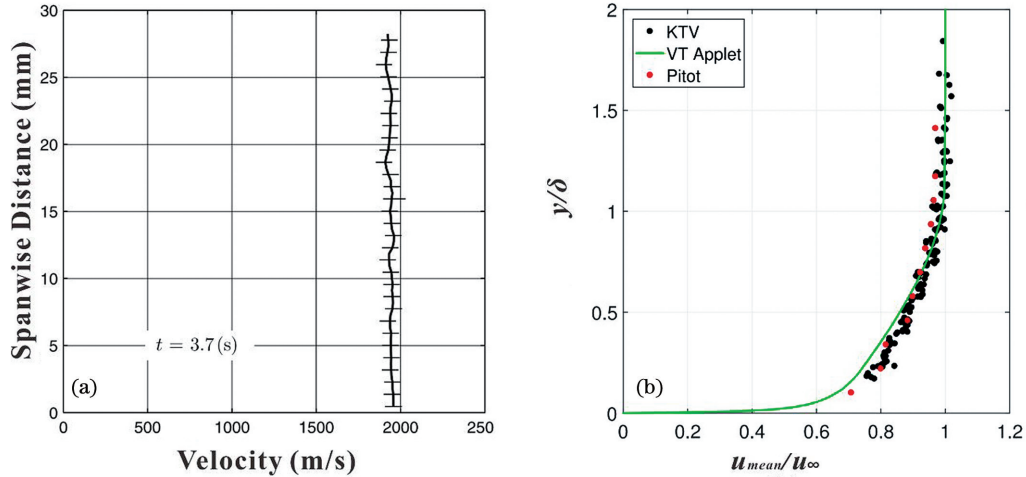


图 20 典型平均速度的剖面图像。(a) 自由来流^[159]; (b) 边界层^[174]

Fig. 20 Profile image of the typical mean velocity. (a) Freestream^[159]; (b) boundary layer^[174]

KTV 技术的主要优势是处于亚稳态的 Kr 具有化学惰性, 不会与流场中其他物质发生化学反应, 目前已实现在高速流场的速度测量。但 KTV 技术需要额外向流场中散布 Kr, 稀释气体组分, 且分子间的碰撞会提高亚稳态 Kr 的淬灭速率, 尤其在高温燃烧场中碰撞淬灭会更剧烈, 使亚稳态 Kr 的寿命更低, 从而降低测速图像的信噪比, 因此, KTV 技术在高温燃烧场的应用还有待进一步研究。

5.3 基于 OH PLIF 的 HTV 测速

羟基分子标记测速 (HTV) 技术以 OH 分子作为示踪分子, 常利用准分子激光光解流场中的水分子产生 OH, 不需要额外散布其他分子。常温常压下光解产生的 OH 寿命为几十 μm ^[177], 而高温环境

Mustafa 等^[159,173] 利用不同激发波长的 PLIF 实现位置读取, 并借助 KTV 技术研究了激波和湍流边界层的相互作用^[174-176], 实现了二维流场速度测量, 无量纲化的边界层平均速度剖面如图 20(b) 所示, 其横、纵坐标分别以平均速度和边界层厚度归一化。

对水分子的光解效率和 OH 浓度有明显增长作用, 因此, HTV 技术可适用于高温场和燃烧场。

Grady 等^[178-179] 利用 HTV 技术在低速非反应流场和燃烧场、火箭尾流场实现速度测量, 并与美国空军实验室合作, 在超燃冲压发动机^[174,180-181] 等高速流场中实现速度测量。在超燃冲压发动机 (2 马赫) 的可压缩流场中, Lahr 等^[180,182] 利用 HTV 技术实现了非反应潮湿空气流的速度测量。标记过程采用多线网格格式标记, 来流速度分别设置为 700、300、200 m/s, 验证了 HTV 技术在亚声速和超声速条件下的测速能力, 图 21(a) 为 700 m/s 时标记的图像。随后, Grady 等^[181] 分别测量了凹腔台阶后、凹腔后斜坡上和支柱尾流区的 HTV 标记图像, 无

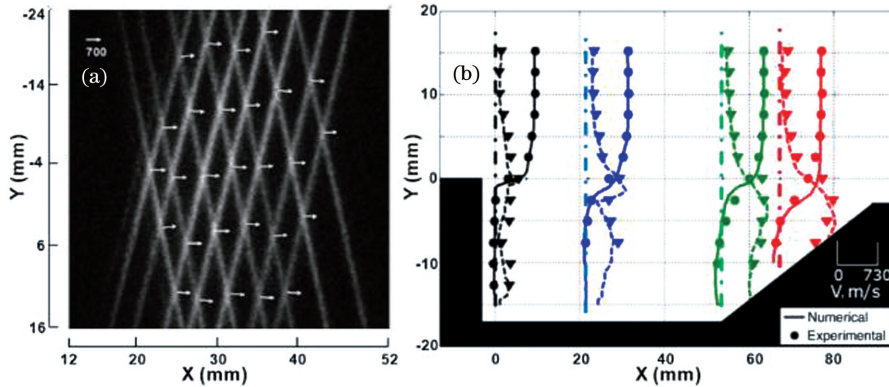


图 21 HTV 图像。(a) 单幅 HTV 图像^[180]; (b) 平均速度和 RMS 波动图像^[181]

Fig. 21 HTV images. (a) Single-shot HTV image^[180]; (b) images of the mean velocity and RMS fluctuation^[181]

支柱条件下的典型图像如图 21(b) 所示,其中点划线为激光标记位置,圆点为平均速度,三角为均方根(RMS)波动。为了实现速度信息的提取,Ramsey 等^[183]提出一种模板匹配方法对 OH 网格进行跟踪,同时确定了线性位移和旋转位移^[40,179,181]。

Ye 等^[40]在双模态超燃冲压发动机中实现了速度测量,典型测速结果如图 22(a) 所示,图 22(a) 和图 22(c) 为非反应流场,图 22(b) 和图 22(d) 为反应流场,测速不确定度为 29 m/s。在非反应流场中,标记信号位置清晰,可直接得到主流区和凹

腔内的速度信息;在燃烧流场中,由于强烈的化学反应覆盖了一部分标记信号,只能获得主流区的速度信息,但 OH 作为标志性的燃烧产物,可以显示已燃区的火焰结构。HTV 技术的标记信号在燃烧场中不可避免地会受到燃烧产物等影响,邵珺等^[184-186]针对提取标记信号、去除背景、降低噪声等开展了一系列工作,可有效提高 HTV 图像的信噪比。胡志云等^[187]提出一种有前景的解决方案,由于光解和燃烧产生 OH 的能级不同,选择合适的 OH 激励线可以抑制燃烧产生的 OH 荧光,有利于提高信噪比。

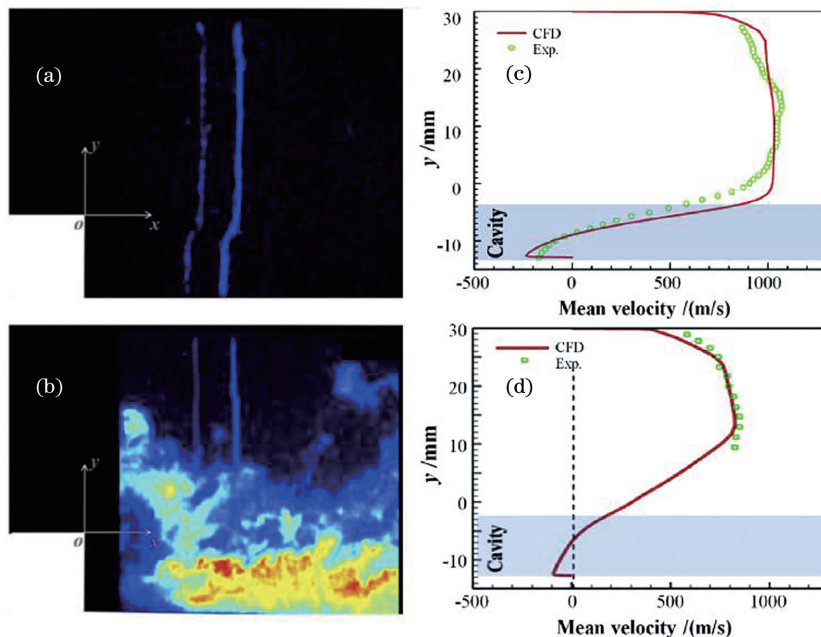


图 22 HTV 图像。(a) 无反应流场的 HTV 图像;(b) 燃烧流场的 HTV 图像;(c) 无反应流场的速度分布;(d) 燃烧流场的速度分布^[40]

Fig. 22 HTV images. (a) HTV image of unreacted flow field; (b) HTV image of combustion flow field; (c) velocity distribution of unreacted flow field; (d) velocity distribution of combustion flow field^[40]

HTV 测速技术可直接利用燃烧产物水分子,不需要额外散布示踪分子,且测速范围较宽,可应用于高温场、燃烧场,具有广阔的应用前景。但燃烧反应产生的高浓度 OH 也会干扰 HTV 信号,对信号提取造成困难。在空间上,PLIF 测速技术目前主要实现一维速度测量以及网格式二维速度测量,借助多台相机及空间重构方法也可以实现三维速度测量^[188]。在时间上,ns-PLIF 可测量的时间尺度已满足超声速流动中物理过程的时间尺度,可认为在单个激光脉冲时间内,流场的流动状态不发生改变,而 ps-PLIF 和 fs-PLIF 测量系统可测量的时间尺度比碰撞和反应的时间尺度更小;随着 kHz 和 MHz 脉冲激光系统的应用,每秒可以获得数千幅连续的测

速图像,提供更高时间分辨的高速气体动力学行为信息,有潜力将测速技术的应用范围从 3D 拓展到“3D+t”,不仅可以获得 3D 速度分布,还可以测得不同时刻的速度变化。

6 发展趋势

在基础湍流燃烧和实际发动机燃烧室中,火焰瞬时结构高速脉动,点火、振荡和熄火等动态过程高速演化,使火焰结构具有显著的三维特征,燃烧和流场强烈耦合,传统的 ~ 10 Hz 量级、二维和单场(组分场或温度场、流场)测量等 PLIF 技术获得的燃烧流场信息依然有限,未来还需将高速 PLIF、体 LIF (VLIF)、PLIF 技术与其他技术相结合实现多场同

步测量发展。

6.1 高速 PLIF

高速 PLIF 技术的发展主要依赖高重频激光器的研制,高重频脉冲串激光器的问世和发展,使 PLIF 技术的测量频率从 ~ 10 Hz 量级提升到 $10\sim 1000$ kHz 量级,高速 PLIF 技术逐步应用于燃烧诊断中捕捉发动机燃烧室点熄火时火焰瞬时结构的高速演化过程。

Hammack 等^[189]利用 10 kHz OH PLIF 技术研究了凹腔稳焰超燃冲压发动机燃烧室火焰瞬时结构的动态演化过程,图 23(a)为 2 马赫超声速来流下乙烯燃料燃烧时火焰的贫燃吹熄过程。Miller 等^[41]利用 100 kHz CH_2O PLIF 观测了 2 马赫超声速来流下乙烯燃料的点火和火焰传播过程,如图 23(b)所示。Allison 等^[79]对超燃冲压发动机燃

烧室中的乙烯预混火焰开展了 50 kHz 的 CH_2O PLIF 研究,观测了火焰预热区结构动态演化过程的时间尺度。Carter 等^[64]在甲烷和空气预混火焰中开展 10 kHz CH PLIF 技术研究,利用 310 \sim 320 nm 范围的 CH (C-X)激发和探测,以较小的激光能量(0.2 mJ)获得较高的信噪比(~ 20)。目前高速 PLIF 的频率最高可达 1 MHz, Jiang 等^[190]在 3 马赫超声速风洞中实现了 1 MHz NO PLIF 测量,用于观测湍流涡旋结构的高速动态变化过程; Peng 等^[30,191]运用 500 Hz OH PLIF 研究了氢气超声速火焰的振荡频率和点熄火过程; Yang 等^[192]运用 20 kHz PLIF 和 PIV 测量了旋流火焰的高温释热区域; Wang 等^[193]利用 20 kHz CH_2O PLIF 研究了声激励作用下的旋流火焰振荡特性。

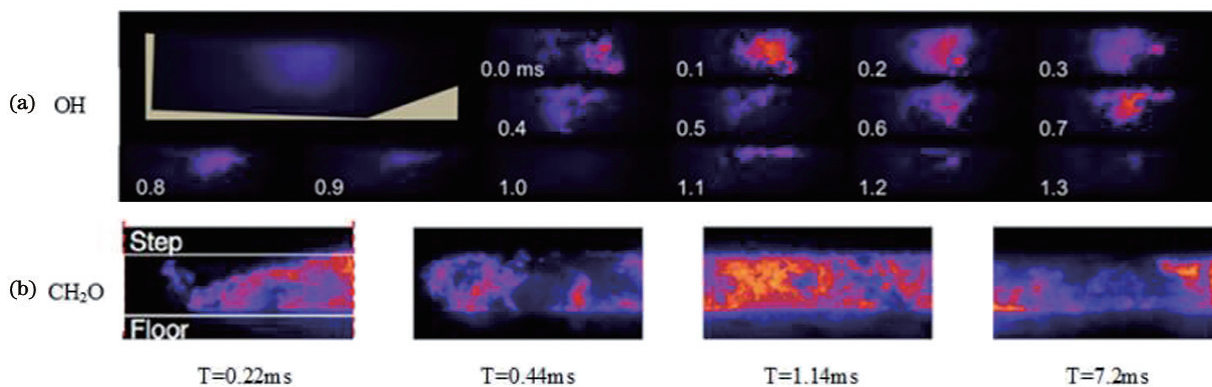


图 23 超燃冲压发动机高速 PLIF 图像。(a) 10 kHz OH PLIF 图像^[189]; (b) 100 kHz CH_2O PLIF 图像^[41]

Fig. 23 High-repetition PLIF images in scramjet engines. (a) 10 kHz OH PLIF images^[189]; (b) 100 kHz CH_2O PLIF images^[41]

高速 PLIF 技术能在 $10\sim 1000$ kHz 范围观测燃烧流场中火焰瞬时结构和流场涡结构的高速动态演化过程,对研究湍流火焰瞬时结构的高速脉动、揭示点熄火和燃烧振荡过程具有重要意义。高速 PLIF 技术能在较短的时间内获得大量实验数据,便于统计分析,极大提高了实验效率。但高速 PLIF 的重复频率、测量时间和测量范围存在矛盾,随着激光重复频率的提高,激光脉冲能量减少,为了保持图像的信噪比,需要缩小激光光片的测量范围;脉冲串激光器能够实现 ~ 100 kHz 重复频率的输出,单个脉冲串的持续时间仅为 $1\sim 10$ ms,两个脉冲串之间的时间间隔为 $5\sim 10$ s。优化脉冲串激光器能量和提高稳定性、发展海量 PLIF 图像的分析处理算法、研制新型高重频激光和实现国产化均是未来高速 PLIF 技术发展的主要方向。

6.2 体激光诱导荧光

VLIF 技术能够将 PLIF 技术的二维测量拓宽为三维测量。VLIF 技术目前尚处于探索阶段,主要应用于重构实验室尺度层流和湍流火焰的三维结构^[43]。Wellander 等^[194]通过改变扫描光片的角度改变激光面,用高速相机进行记录并进行图像叠加,对火焰的 OH 基实现了 3D+t 的解析,其实验原理和 OH 分布重构图像如图 24 所示。

Xu 等^[195]利用光学镜片形成体激光,再从五个视角拍摄火焰中的自由基图像,通过空间重构,获得 CH 自由基的三维分布,VLIF 测量方案如图 25(a)所示,其三维火焰重构图像如图 25(b)所示。Ma 等^[43]运用甲烷预混火焰实现了尺寸为 $9.3\text{ mm}\times 9.3\text{ mm}\times 32.7\text{ mm}$ 的 CH 基 VLIF 测量,通过对比三维重构火焰的投影图像与单一视角拍摄的图像,测得三维重构火焰的误差在 0.02 mm 以内。

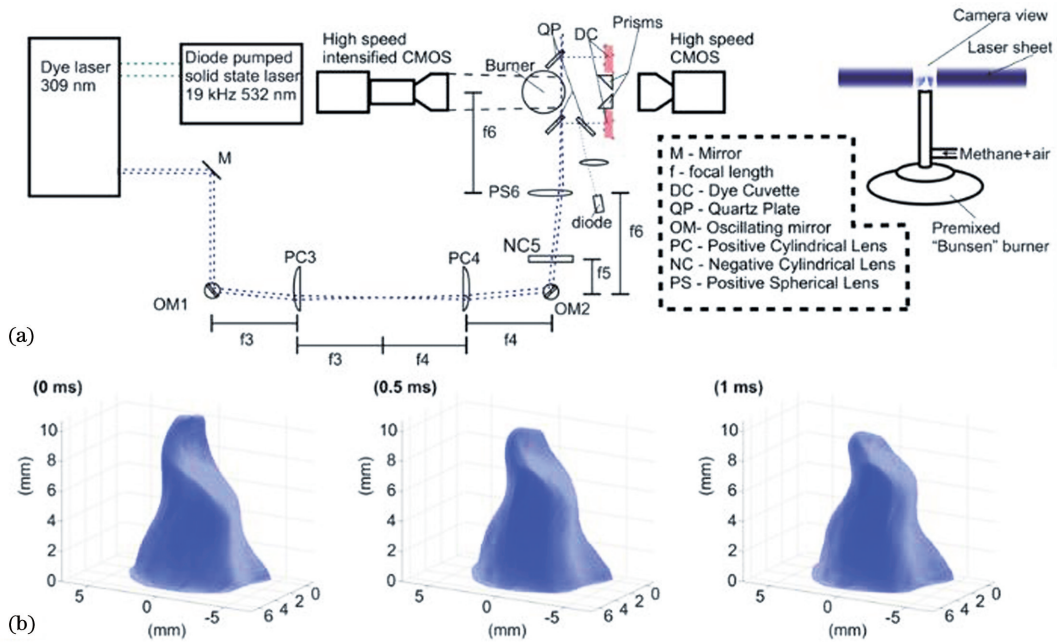


图 24 火焰结构的 3D 重构。(a)实验示意图；(b)OH 基的 3D 重构^[194]

Fig. 24 3D reconstruction of the flame structure. (a) Experimental schematic diagram; (b) 3D reconstruction of the OH radicals^[194]

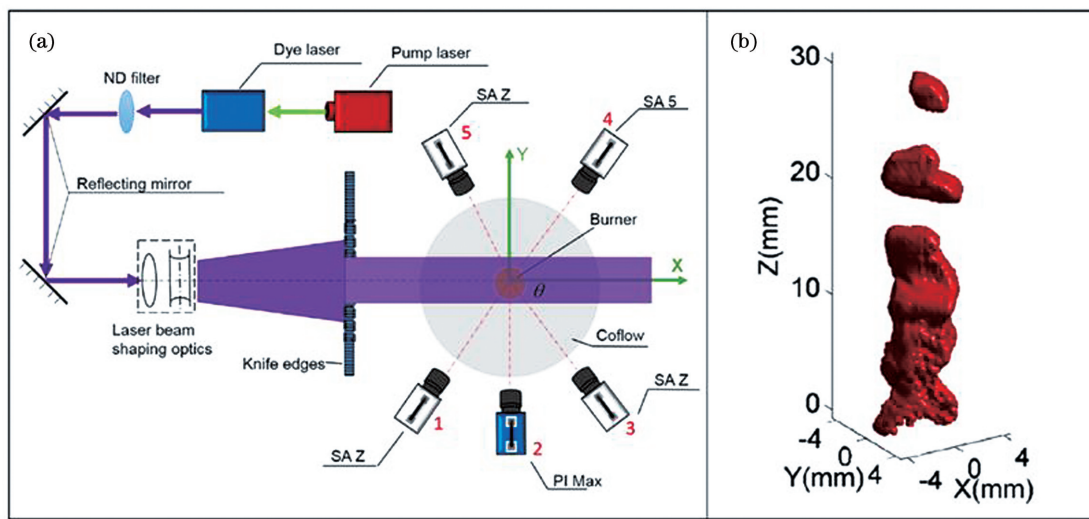


图 25 VLIF 技术。(a)实验装置示意图；(b)火焰 CH 基三维重构^[195]

Fig. 25 VLIF technique. (a) Schematic of the experimental setup; (b) three-dimensional reconstruction of the CH radicals in a flame^[195]

Halls 等^[196]对抬升火焰的 OH 基进行了 VLIF 测量。通过四分幅相机耦合 ICCD 相机进行八个平面的 OH 基分布,实现了抬升火焰尺寸为 40 mm × 35 mm × 55 mm 的 OH 基 VLIF 测量。

相比 PLIF, VLIF 技术的优点在于能提供火焰的三维信息或 3D+t 解析,未来可能实现多组分的 VLIF 同步测量^[44],但目前 VLIF 技术的测量范围很小,无法实现大范围的立体观测^[197]。VLIF 技术实现难度较大,其光路和相机布置需经过精确计

算^[195]。同时,火焰重构算法的标准不统一,火焰重建时难以精确估计误差^[195]。超声速火焰分布范围广、脉动性强、三维结构复杂,对开展高速 VLIF 诊断具有迫切需求^[198]。但将 VLIF 技术用于观测超燃冲压发动机的三维火焰结构还存在困难,需要广阔的观测视野和复杂的光路布局,全透明光学玻璃燃烧室^[71]未来可能会满足 VLIF 所需的多视角诊断需求。

6.3 多场同步测量

PLIF 技术与粒子成像测速 (PIV)、瑞利散射等

非接触激光诊断技术相结合可实现组分场、流场、温度场等多场同步测量^[199]。目前主要应用于 PLIF/PIV 同步测组分和速度场^[180,200]、PLIF/瑞利散射同步测组分和温度场^[201-202]。

PLIF/PIV 同步测量方面, Fugger 等^[46,203]开展了 10 kHz OH/CH₂O PLIF 和 PIV 同步测量, 对火焰的预热区、反应区和速度场进行成像, 测量结果如图 26(a)所示。Boxx 等^[200]对燃气轮机燃烧室中的贫燃预混火焰进行了 kHz 级 OH PLIF 和 PIV 同步测量, 实验结果如图 26(b)所示, 获得了燃烧室速度场和释热率的动态变化过程。Chtereve 等^[45]针对旋流燃烧室开展了 5 kHz OH PLIF、煤油 PLIF 和 SPIV 同步测量, 获得了火焰产物区、煤油分布和速

度场的瞬时结构和相对位置分布, 实验结果如图 26(c)所示。Skiba 等^[204]利用多组分 PLIF 和 PIV 对湍流预混火焰的瞬时结构和速度分布进行高频(20 kHz)同步观测, 通过实验证实了湍流涡旋结构可以拓宽火焰前缘。Weinkauff 等^[205]结合 10 kHz 的 SPIV 和丙酮 PLIF 研究了射流火焰的速度场和燃料混合过程。Hammack 等^[206-207]利用 C-X(0,0)谱线实现了 CH PLIF 和 PIV 的同步拍摄。Gao 等^[208]运用 10 kHz PIV 和 CH₂O PLIF 研究了火焰的热声振荡特性。Guo 等^[209-210]采用同步 OH PLIF 和 PIV 技术研究了氢气助燃下的贫燃预混火焰燃烧特性。Fan 等^[211]利用同步 PIV 和煤油 PLIF 技术研究了旋流燃烧室的流场结构和煤油分布特性。

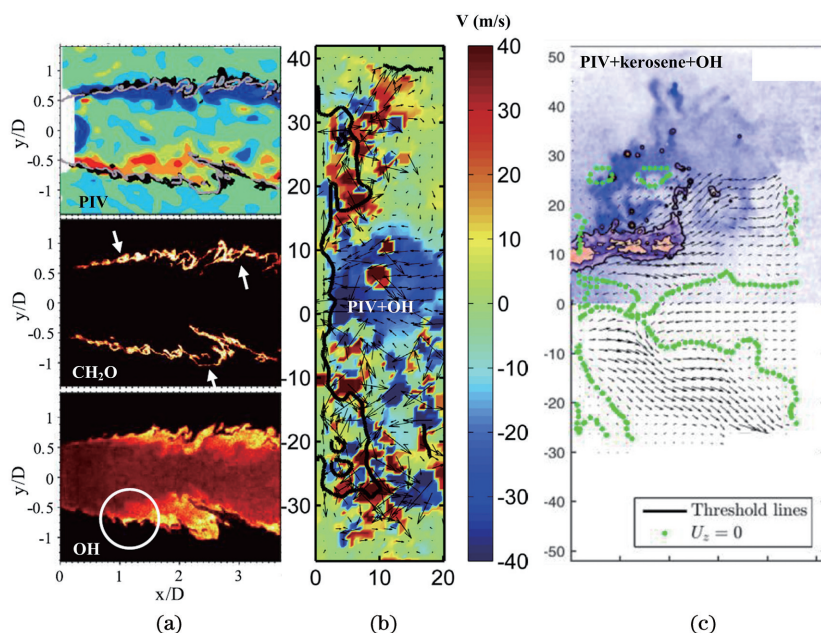


图 26 PLIF/PIV 同步测量图像。(a) 钝体火焰 PIV、CH₂O PLIF 和 OH PLIF 图像^[46]; (b) 抬举火焰 PIV、OH PLIF 图像^[200]; (c) 旋流火焰 PIV、煤油 PLIF、OH PLIF 图像^[45]

Fig. 26 Simultaneous measurement images of PLIF/PIV. (a) PIV and CH₂O/OH PLIF images for the bluff body flame^[46]; (b) PIV and OH PLIF images for the lifted flame^[200]; (c) PIV, kerosene PLIF and OH PLIF images for the swirling flame^[45]

在 PLIF/瑞利散射同步测量方面, Chtereve 等^[212]实现了 10 kHz OH/CH₂O PLIF 和瑞利散射的同步测量, 获得了火焰瞬时结构和火焰温度图像, 结果如图 27(a)所示。Skiba 等^[213]用 CH/OH PLIF 和瑞利散射进行同步测温, 结果如图 27(b)所示, 获得了火焰已燃区、反应区和火焰温度的相对位置分布信息。Kong 等^[214]运用 CH₂O/CH PLIF 和瑞利散射研究了等离子体辅助甲烷预混火焰燃烧机理, 结果如图 27(c)所示, 发现了等离子体所产生的高温区域附近 CH₂O 基信号较弱, CH₂O 基主要分

布于低温的燃料分解区。Novoselo 等^[215]结合丙酮 PLIF、CH₂O PLIF 和平面瑞利散射对湍流冷火焰进行了化学动力学分析。Ge 等^[216]将二维瑞利散射获得的主要释热区域与通过 OH PLIF 获得的主要反应区域相结合, 研究了旋流火焰的燃烧特性。

除了 PLIF/PIV 和 PLIF/瑞利散射同步测量外, PLIF 技术还能与其他非接触式光学测量技术相结合实现燃烧流场的多场、多参数测量。PLIF 技术与纹影技术结合使用有助于研究超声速燃烧的动态过程, Do 等^[217]利用纹影技术与 OH PLIF 技术研

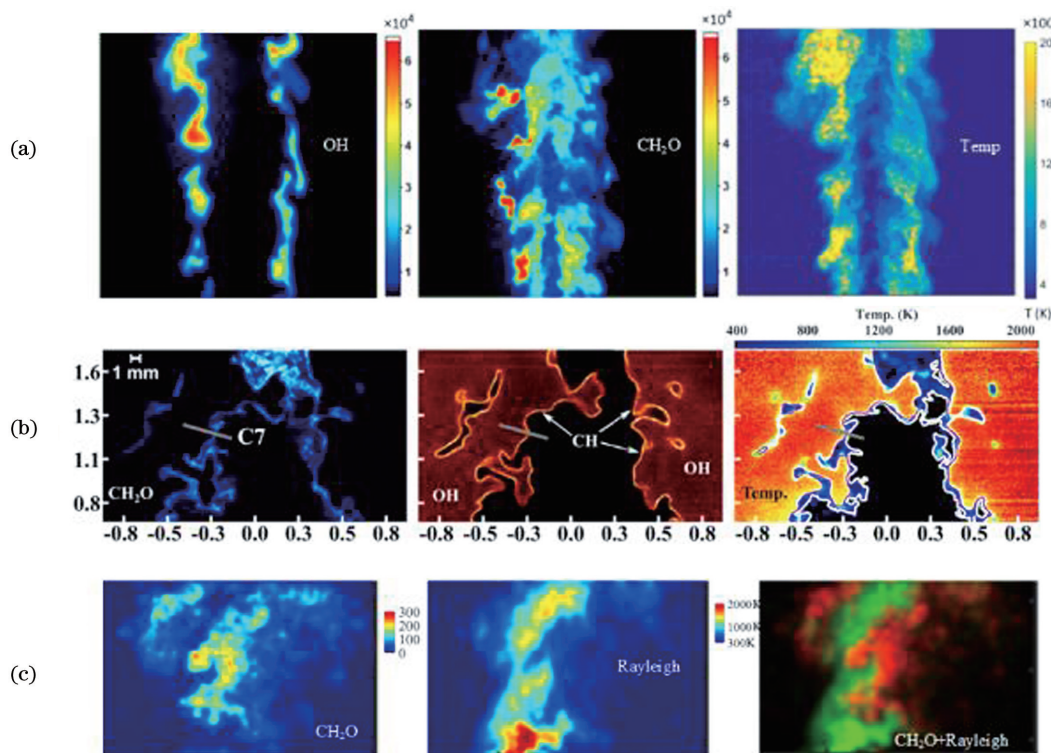


图 27 PLIF 和瑞利散射同步测量图像。(a) OH/CH₂O PLIF 和瑞利散射图像^[212]; (b) CH₂O/OH/CH PLIF 和瑞利散射图像^[213]; (c) CH₂O PLIF 和瑞利散射图像^[214]

Fig. 27 Simultaneous measurement images of PLIF and Rayleigh scattering. (a) OH/CH₂O PLIF and Rayleigh scattering images^[212]; (b) CH₂O/OH/CH PLIF and Rayleigh scattering images^[213]; (c) CH₂O PLIF and Rayleigh scattering images^[214]

究了 ns 脉冲等离子体强化超声速燃烧的效果和机理。PLIF 技术与平面激光诱导发光 (PLII) 技术用于研究碳烟的形成, Jain 等^[218] 运用 OH PLIF 技术和 PLII 技术研究了 H 原子浓度对于碳烟形成的影响规律。Guiberti 等^[219] 实现了 CH₂O PLIF、OH PLIF、CH₄ 拉曼散射和 PIV 的同步测量, 对抬升射流火焰的未燃区、已燃区、当量比和速度场进行了同步测量。Liu 等^[220] 利用 PLIF 技术和激光诱导击穿光谱 (LIBS) 技术, 研究了生物质燃料燃烧过程中的钾释放过程和影响因素。

多场同步测量有助于将同时获得的组分场、流场和温度场等综合信息进行对比研究, 但实验系统复杂, 时序同步、空间合束等操作难度大, 多束激光的使用可能带来额外的杂散光, 降低图像的信噪比。受限于光路调节的难度和实验系统的复杂性, 多场同步测量主要应用于实验室尺度基础层流和湍流火焰的诊断, 随着激光诊断技术的不断发展和完善, 多场同步测量技术有望应用于发动机燃烧流场的诊断, 将组分场与速度场、温度场等其他物理量进行同时测量, 以获得发动机燃烧室的多参数综合信息, 为

发动机燃烧室的优化设计提供支撑。

PLIF 技术可应用于固体颗粒或碳烟颗粒的燃烧诊断中。Park 等^[221] 运用 Kr PLIF、PIV 和 LII 同步测量了湍流非预混火焰中碳烟颗粒的耗散率和体积分数, 碳烟颗粒的散射光可被窄带滤波片过滤。Köser 等^[222] 运用 PLIF 对比自发辐射研究了单个煤颗粒的燃烧过程, 相比自发辐射, OH PLIF 更有利于研究煤颗粒内部的燃烧过程。Balusamy 等^[223] 运用米散射和 OH PLIF 技术研究了煤颗粒的燃烧过程。煤颗粒和燃烧中碳烟颗粒的米散射会对 PLIF 信号造成干扰, 使用窄带滤波片并调整相机延迟可以有效降低信号干扰。

PLIF 技术还可用于诊断液态燃料的燃烧, Wang 等^[224] 针对超声速火焰实现了煤油 PLIF 和 OH PLIF 的同步测量, 在测量 OH PLIF 时激光诱导煤油和其他大分子会产生 PAH 信号。Malbois 等^[225] 利用 10 kHz OH PLIF 和 PIV 研究了煤油旋流火焰的 OH 基分布和速度场, 拍摄 OH PLIF 时发现燃烧室入口附近的大尺寸煤油液滴具有较强的米散射。激光诱导液态燃料产生的荧光可能会干扰

目标粒子的荧光,且激光穿过液滴时会发生散射,导致激光在平面上分布不均匀,对定量分析产生影响,因此需要根据激光强度分布对荧光信号进行校正^[224]。

7 结论与展望

LIF 技术作为研究燃烧的重要测量手段,具有非扰动、实时原位测量、组分选择性强、灵敏度好、时空分辨率高等优势,多组分 PLIF 技术、示踪 PLIF 技术、基于 PLIF 的 MTV 技术已经广泛应用于燃烧诊断中测量火焰瞬时结构、组分浓度、温度和流场速度等重要特征参数。

PLIF 技术能够通过成像燃烧过程中 CH_2O 、OH 和 CH 等重要组分的二维分布,实现对发动机燃烧室火焰预热区、已燃区和反应区瞬时结构的高时空分辨可视化;通过加入丙酮、甲苯等示踪物质显示发动机混合场组分浓度和温度等重要信息,TLAF 能测量火焰温度的二维分布;MTV 技术利用 PLIF 实现读的功能,从而测量冷流场和燃烧场中的流速分布,测量范围从低速拓宽到高超声速。尽管 LIF 技术在燃烧诊断中已经取得重要研究进展,但存在着重复频率低(~ 10 Hz)、维度少(2D)、单场测量等问题。

随着高能高重频脉冲激光器的发展,高速 PLIF 技术($10\sim 1000$ kHz)逐步应用于燃烧诊断中测量点熄火、燃烧振荡等过程中火焰瞬时结构的动态演化。VLIF 技术在开敞空间的火焰炉中已经被演示验证,能够成像火焰的三维结构,且与高速激光器结合能实现 4D(3D+t)测量,未来有望应用于成像发动机燃烧室火焰三维瞬时结构的高速演化过程。PLIF 技术与 PIV、瑞利散射等技术同步使用,能实现组分场/流场/温度场的多场、多参数同步可视化,有助于进一步揭示燃烧与湍流相互作用机理。VLIF 技术和多场多参数同步诊断技术目前主要应用于基础燃烧诊断,但还需要解决复杂光路调节和光学视窗设计、燃烧室壁面杂散光滤除、信噪比优化等问题。

仅依靠 LIF 技术获得的发动机燃烧流场信息依然有限,PLIF 测量结果需要更好地结合理论模型和数值模拟结果,才能进一步揭示发动机混合、流动、燃烧的特性和机理,为发动机燃烧室的优化设计奠定基础,为提高发动机燃烧效率和推力性能提供支撑。

参 考 文 献

- [1] Ju Y G, Sun W T. Plasma assisted combustion: dynamics and chemistry[J]. *Progress in Energy and Combustion Science*, 2015, 48: 21-83.
- [2] Feng R, Zhu J J, Wang Z G, et al. Dynamic characteristics of a gliding arc plasma-assisted ignition in a cavity-based scramjet combustor [J]. *Acta Astronautica*, 2020, 171: 238-244.
- [3] Sun M B, Wang H B, Cai Z, et al. Unsteady supersonic combustion [M]. Singapore: Springer Singapore, 2020.
- [4] Bai X, Cheng P, Li Q L, et al. Effects of self-pulsation on combustion instability in a liquid rocket engine[J]. *Experimental Thermal and Fluid Science*, 2020, 114: 110038.
- [5] Urbano A, Selle L, Staffelbach G, et al. Exploration of combustion instability triggering using large eddy simulation of a multiple injector liquid rocket engine [J]. *Combustion and Flame*, 2016, 169: 129-140.
- [6] Stamatis A, Mathioudakis K, Papailiou K D. Adaptive simulation of gas turbine performance[J]. *Journal of Engineering for Gas Turbines & Power*, 1990, 112(2): 168-175.
- [7] Valera-Medina A, Marsh R, Runyon J, et al. Ammonia-methane combustion in tangential swirl burners for gas turbine power generation[J]. *Applied Energy*, 2017, 185: 1362-1371.
- [8] Malé Q, Staffelbach G, Vermorel O, et al. Large eddy simulation of pre-chamber ignition in an internal combustion engine[J]. *Flow, Turbulence and Combustion*, 2019, 103(2): 465-483.
- [9] Wu J, Chen L H, Zhou J W, et al. Effects of fuel types on soot evolution in diffusion flames [J]. *Chinese Journal of Lasers*, 2019, 46(4): 0411001. 吴建, 陈玲红, 周剑武, 等. 扩散火焰中燃料种类对碳烟演变过程的影响[J]. *中国激光*, 2019, 46(4): 0411001.
- [10] Wang Z G, Yang Y X, Liang J H, et al. Analysis and modeling of blowout limits of cavity flame in supersonic flows[J]. *Scientia Sinica: Technologica*, 2014, 44(9): 961-972. 王振国, 杨揖心, 梁剑寒, 等. 超声速气流中稳焰凹腔吹熄极限分析与建模[J]. *中国科学: 技术科学*, 2014, 44(9): 961-972.
- [11] Yang Y X, Wang Z G, Sun M B, et al. Empirical mixing model of transverse gaseous jet in supersonic flow[J]. *Journal of Aerospace Power*, 2015, 30(6): 1391-1399. 杨揖心, 王振国, 孙明波, 等. 超声速气流中横向气体射流混合经验模型[J]. *航空动力学报*, 2015, 30

- (6): 1391-1399.
- [12] Zhang Y X, Wang Z G, Sun M B, et al. An investigation on one-dimensional model of heat release distribution in scramjet combustor [J]. *Journal of Propulsion Technology*, 2015, 36(12): 1852-1858.
张雁翔, 王振国, 孙明波, 等. 超燃燃烧室一维释热分布模型研究[J]. *推进技术*, 2015, 36(12): 1852-1858.
- [13] Wu J S, Wang Z G, Bai X S, et al. The hybrid RANS/LES of partially premixed supersonic combustion using G/Z flamelet model [J]. *Acta Astronautica*, 2016, 127: 375-383.
- [14] Li P B, Wang Z G, Bai X S, et al. Three-dimensional flow structures and droplet-gas mixing process of a liquid jet in supersonic crossflow [J]. *Aerospace Science and Technology*, 2019, 90: 140-156.
- [15] Hu Z Y, Liu J R, Zhang Z R, et al. The research progress of laser combustion diagnostics techniques and applications[J]. *Engineering Sciences*, 2009, 11(11): 45-50.
胡志云, 刘晶儒, 张振荣, 等. 激光燃烧诊断技术及应用研究进展[J]. *中国工程科学*, 2009, 11(11): 45-50.
- [16] Yang B, He G Q, Liu P J, et al. TDLAS-based measurements of parameters for incoming flow hot-firing test of air-breathing rocket engine[J]. *Chinese Journal of Lasers*, 2011, 38(5): 0508006.
杨斌, 何国强, 刘佩进, 等. 利用 TDLAS 技术开展吸气式发动机来流热试实验参数测量[J]. *中国激光*, 2011, 38(5): 0508006.
- [17] Liu X C, Li Y Y, Zhou Z Y, et al. Applications of laser spectroscopy and mass spectrometry in combustion diagnostics[J]. *Journal of Experiments in Fluid Mechanics*, 2016, 30(1): 43-54, 67.
刘训臣, 李玉阳, 周忠岳, 等. 光谱法和取样分析法在燃烧诊断研究中的应用[J]. *实验流体力学*, 2016, 30(1): 43-54, 67.
- [18] Ehn A, Zhu J J, Li X S, et al. Advanced laser-based techniques for gas-phase diagnostics in combustion and aerospace engineering[J]. *Applied Spectroscopy*, 2017, 71(3): 341-366.
- [19] Zhang B Q, Xu Z Y, Liu J G, et al. Absorption model of wavelength modulation spectroscopy in combustion flow field[J]. *Chinese Journal of Lasers*, 2019, 46(7): 0711001.
张步强, 许振宇, 刘建国, 等. 燃烧流场波长调制光谱吸收模型的研究[J]. *中国激光*, 2019, 46(7): 0711001.
- [20] Peng Y Q, Kan R F, Xu Z Y, et al. Measurement of CO concentration in combustion field based on mid-infrared absorption spectroscopy[J]. *Chinese Journal of Lasers*, 2018, 45(9): 0911010.
彭于权, 阚瑞峰, 许振宇, 等. 基于中红外吸收光谱技术的燃烧场 CO 浓度测量研究[J]. *中国激光*, 2018, 45(9): 0911010.
- [21] Kan R F, Xia H H, Xu Z Y, et al. Research and progress of flow field diagnosis based on laser absorption spectroscopy [J]. *Chinese Journal of Lasers*, 2018, 45(9): 0911005.
阚瑞峰, 夏晖晖, 许振宇, 等. 激光吸收光谱流场诊断技术应用研究与进展[J]. *中国激光*, 2018, 45(9): 0911005.
- [22] Aldén M, Bood J, Li Z S, et al. Visualization and understanding of combustion processes using spatially and temporally resolved laser diagnostic techniques [J]. *Proceedings of the Combustion Institute*, 2011, 33(1): 69-97.
- [23] Kychakoff G, Howe R D, Hanson R K, et al. Quantitative visualization of combustion species in a plane[J]. *Applied Optics*, 1982, 21(18): 3225-3227.
- [24] Zhang J F, Chen L H, Yu J H, et al. Detection of polycyclic aromatic hydrocarbons in diffusion flame of propane by laser induced fluorescence [J]. *Chinese Journal of Lasers*, 2020, 47(4): 0411002.
张健夫, 陈玲红, 余佳涵, 等. 丙烷扩散火焰中多环芳烃的激光诱导荧光测量研究[J]. *中国激光*, 2020, 47(4): 0411002.
- [25] Zhou B, Brackmann C, Li Z S, et al. Simultaneous multi-species and temperature visualization of premixed flames in the distributed reaction zone regime[J]. *Proceedings of the Combustion Institute*, 2015, 35(2): 1409-1416.
- [26] Gao J L, Kong C D, Zhu J J, et al. Visualization of instantaneous structure and dynamics of large-scale turbulent flames stabilized by a gliding arc discharge [J]. *Proceedings of the Combustion Institute*, 2019, 37(4): 5629-5636.
- [27] Lü L, Tan J G, Zhu J J. Visualization of the heat release zone of highly turbulent premixed jet flames [J]. *Acta Astronautica*, 2017, 139: 258-265.
- [28] Li X P, Liu W D, Pan Y, et al. Characterization of kerosene distribution around the ignition cavity in a scramjet combustor [J]. *Acta Astronautica*, 2017, 134: 11-16.
- [29] Li X P, Liu W D, Yang L C, et al. Experimental investigation on fuel distribution in a scramjet combustor with dual cavity[J]. *Journal of Propulsion and Power*, 2017, 34(2): 552-556.
- [30] Peng J B, Cao Z, Yu X, et al. Analysis of combustion instability of hydrogen fueled scramjet

- combustor on high-speed OH-PLIF measurements and dynamic mode decomposition [J]. *International Journal of Hydrogen Energy*, 2020, 45(23): 13108-13118.
- [31] Wu G, Li Y, Wan M G, et al. Visualization of flame structure in supersonic combustion by planar laser induced fluorescence technique [J]. *Journal of Experiments in Fluid Mechanics*, 2020, 34(3): 70-77.
吴戈, 李韵, 万明罡, 等. 平面激光诱导荧光技术在超声速燃烧火焰结构可视化中的应用[J]. *实验流体力学*, 2020, 34(3): 70-77.
- [32] Zhu J J, Zhao G Y, Long T H, et al. Simultaneous OH and CH₂O PLIF imaging of flame structures[J]. *Journal of Experiments in Fluid Mechanics*, 2016, 30(5): 55-60, 87.
朱家健, 赵国焱, 龙铁汉, 等. OH 和 CH₂O 平面激光诱导荧光同时成像火焰结构[J]. *实验流体力学*, 2016, 30(5): 55-60, 87.
- [33] Chen S, Kapsta L, Weng W B, et al. Simultaneous multi-species PLIF diagnostic on CH₄-air inverse diffusion jet flame [J]. *Journal of Experiments in Fluid Mechanics*, 2018, 32(1): 26-32.
陈爽, Kapsta J L, 翁武斌, 等. CH₄/air 反扩散射流火焰多组分同步 PLIF 诊断[J]. *实验流体力学*, 2018, 32(1): 26-32.
- [34] Yan H, Zhang S H, Yu X L, et al. Flame structure and dynamics characters investigation by OH and CH₂O planar laser-induced fluorescence in the swirl combustor[J]. *Journal of Aerospace Power*, 2019, 34(4): 894-907.
严浩, 张少华, 余西龙, 等. OH 与 CH₂O 双组分平面激光诱导荧光对旋流燃烧室火焰结构与脉动特征的研究[J]. *航空动力学报*, 2019, 34(4): 894-907.
- [35] Vena P C, Deschamps B, Guo H S, et al. Heat release rate variations in a globally stoichiometric, stratified iso-octane/air turbulent V-flame [J]. *Combustion and Flame*, 2015, 162(4): 944-959.
- [36] Chen S, Su T, Li Z S, et al. Quantitative measurement of hydroxyl radical (OH) concentration in premixed flat flame by combining laser-induced fluorescence and direct absorption spectroscopy[J]. *Chinese Physics B*, 2016, 25(10): 100701.
- [37] Medwell P R, Chan Q N, Kalt P A M, et al. Development of temperature imaging using two-line atomic fluorescence [J]. *Applied Optics*, 2009, 48(6): 1237-1248.
- [38] Zhang Z R, Huang M S, Hu Z Y, et al. Measurement of CH₄/AIR flame parameters by combination of laser induced polarization spectroscopy and laser induced fluorescence techniques [J]. *High Power Laser and Particle Beams*, 2013, 25(11): 2821-2825.
张振荣, 黄梅生, 胡志云, 等. 基于激光诱导偏振光谱与激光诱导荧光技术的 CH₄/AIR 火焰参数测量[J]. *强激光与粒子束*, 2013, 25(11): 2821-2825.
- [39] Borggren J, Burns I S, Sahlberg A L, et al. Temperature imaging in low-pressure flames using diode laser two-line atomic fluorescence employing a novel indium seeding technique[J]. *Applied Physics B*, 2016, 122(3): 1-8.
- [40] Ye J F, Shi D Y, Song W Y, et al. Investigation of turbulence flow characteristics in a dual-mode scramjet combustor using hydroxyl tagging velocimetry[J]. *Acta Astronautica*, 2019, 157: 276-281.
- [41] Miller J D, Peltier S J, Slipchenko M N, et al. Investigation of transient ignition processes in a model scramjet pilot cavity using simultaneous 100 kHz formaldehyde planar laser-induced fluorescence and CH^{*} chemiluminescence imaging[J]. *Proceedings of the Combustion Institute*, 2017, 36(2): 2865-2872.
- [42] Li X D, Mei F, Yan R P, et al. Review of burst-mode lasers for high-speed PLIF imaging diagnostics [J]. *Optics and Precision Engineering*, 2019, 27(10): 2116-2126.
李旭东, 梅峰, 闫仁鹏, 等. 高速 PLIF 成像诊断应用的脉冲串激光器研究进展[J]. *光学精密工程*, 2019, 27(10): 2116-2126.
- [43] Ma L, Lei Q C, Ikeda J, et al. Single-shot 3D flame diagnostic based on volumetric laser induced fluorescence (VLIF) [J]. *Proceedings of the Combustion Institute*, 2017, 36(3): 4575-4583.
- [44] Halls B R, Gord J R, Hsu P S, et al. Development of two-color 3D tomographic VLIF measurements [C]// 2018 AIAA Aerospace Sciences Meeting, January 8-12, 2018, Kissimmee, Florida. Reston, Virginia: AIAA, 2018.
- [45] Chterevev I, Rock N, Ek H, et al. Simultaneous high speed (5 kHz) fuel-PLIE, OH-PLIF and stereo PIV imaging of pressurized swirl-stabilized flames using liquid fuels [C] // 55th AIAA Aerospace Sciences Meeting, January 9-13, 2017, Grapevine, Texas. Reston, Virginia: AIAA, 2017.
- [46] Fugger C A, Yi T, Sykes J, et al. The structure and dynamics of a bluff-body stabilized premixed reacting flow [C] // 2018 AIAA Aerospace Sciences Meeting, January 8-12, 2018, Kissimmee, Florida. Reston, Virginia: AIAA, 2018.
- [47] Eckbreth A C. Laser diagnostics for combustion temperature and species[M]//Culick F, Heitor M V, Whitelaw J H, et al. *Unsteady Combustion*. NATO

- ASI Series (Series E: Applied Sciences). Dordrecht: Springer, 1996, 306: 393-410.
- [48] Borggren J. Two-line atomic fluorescence for thermometry in reactive flows [D]. Lund, Sweden: Lund University, 2018.
- [49] Kaminski C F, Hult J, Aldén M. High repetition rate planar laser induced fluorescence of OH in a turbulent non-premixed flame [J]. Applied Physics B, 1999, 68(4): 757-760.
- [50] Bergthorson J M, Goodwin D G, Dimotakis P E. Particle streak velocimetry and CH laser-induced fluorescence diagnostics in strained, premixed, methane-air flames [J]. Proceedings of the Combustion Institute, 2005, 30(1): 1637-1644.
- [51] Tanahashi M, Murakami S, Choi G M, et al. Simultaneous CH-OH PLIF and stereoscopic PIV measurements of turbulent premixed flames [J]. Proceedings of the Combustion Institute, 2005, 30(1): 1665-1672.
- [52] Li Z S, Kiefer J, Zetterberg J, et al. Development of improved PLIF CH detection using an Alexandrite laser for single-shot investigation of turbulent and lean flames [J]. Proceedings of the Combustion Institute, 2007, 31(1): 727-735.
- [53] Carter C D, Hammack S D, Lee T. High-speed planar laser-induced fluorescence of the CH radical using the $C^2\Sigma^+ - X^2\Pi(0, 0)$ band [J]. Applied Physics B Photophysics and Laser Chemistry, 2014, 116(3): 515-519.
- [54] Li Z S, Li B, Sun Z W, et al. Turbulence and combustion interaction: high resolution local flame front structure visualization using simultaneous single-shot PLIF imaging of CH, OH, and CH₂O in a piloted premixed jet flame [J]. Combustion and Flame, 2010, 157(6): 1087-1096.
- [55] Harrington J E, Smyth K C. Laser-induced fluorescence measurements of formaldehyde in a methane/air diffusion flame [J]. Chemical Physics Letters, 1993, 202(3/4): 196-202.
- [56] Zhou B, Kiefer J, Zetterberg J, et al. Strategy for PLIF single-shot HCO imaging in turbulent methane/air flames [J]. Combustion and Flame, 2014, 161(6): 1566-1574.
- [57] Zhou B, Brackmann C, Li Z S, et al. Development and application of CN PLIF for single-shot imaging in turbulent flames [J]. Combustion and Flame, 2015, 162(2): 368-374.
- [58] Lee T, Jeffries J B, Hanson R K. Experimental evaluation of strategies for quantitative laser-induced-fluorescence imaging of nitric oxide in high-pressure flames (1 - 60 bar) [J]. Proceedings of the Combustion Institute, 2007, 31(1): 757-764.
- [59] Kulatilaka W D, Patterson B D, Frank J H, et al. Comparison of nanosecond and picosecond excitation for interference-free two-photon laser-induced fluorescence detection of atomic hydrogen in flames [J]. Applied Optics, 2008, 47(26): 4672-4683.
- [60] Frank J H, Chen X L, Patterson B D, et al. Comparison of nanosecond and picosecond excitation for two-photon laser-induced fluorescence imaging of atomic oxygen in flames [J]. Applied Optics, 2004, 43(12): 2588-2597.
- [61] Zhou B, Brackmann C, Wang Z K, et al. Thin reaction zone and distributed reaction zone regimes in turbulent premixed methane/air flames: scalar distributions and correlations [J]. Combustion and Flame, 2017, 175: 220-236.
- [62] Wang J H, Yu Q Q, Zhang W J, et al. Development of a turbulence scale controllable burner and turbulent flame structure analysis [J]. Experimental Thermal and Fluid Science, 2019, 109: 109898.
- [63] Li B, Zhang D Y, Yao M F, et al. Strategy for single-shot CH₃ imaging in premixed methane/air flames using photofragmentation laser-induced fluorescence [J]. Proceedings of the Combustion Institute, 2017, 36(3): 4487-4495.
- [64] Carter C D, Hammack S, Lee T. High-speed flamefront imaging in premixed turbulent flames using planar laser-induced fluorescence of the CH C-X band [J]. Combustion and Flame, 2016, 168: 66-74.
- [65] Li B, Li X F, Yao M F, et al. Methyl radical imaging in methane-air flames using laser photofragmentation-induced fluorescence [J]. Applied Spectroscopy, 2015, 69(10): 1152-1156.
- [66] Wang H B, Wang Z G, Sun M B, et al. Combustion characteristics in a supersonic combustor with hydrogen injection upstream of cavity flameholder [J]. Proceedings of the Combustion Institute, 2013, 34(2): 2073-2082.
- [67] Gamba M, Mungal M G. Ignition, flame structure and near-wall burning in transverse hydrogen jets in supersonic crossflow [J]. Journal of Fluid Mechanics, 2015, 780: 226-273.
- [68] Cantu L M L, Gallo E C A, Cutler A D, et al. OH PLIF visualization of a premixed ethylene-fueled dual-mode scramjet combustor [C] // 54th AIAA Aerospace Sciences Meeting, January 4-8, 2016, San Diego, California, USA. Reston, Virginia: AIAA, 2016.
- [69] Geipel C M, Rockwell R D, Chelliah H K, et al. High-spatial-resolution OH PLIF visualization in a cavity-stabilized ethylene-air turbulent flame [C] // 33rd AIAA Aerodynamic Measurement Technology

- and Ground Testing Conference, June 5-9, 2017, Denver, Colorado, USA. Reston, Virginia: AIAA, 2017.
- [70] Geipel C M, Cutler A D, Rockwell R D, et al. Characterization of flame front structure in a dual-mode scramjet combustor with OH-PLIF[C]//AIAA Scitech 2019 Forum, January 7-11, 2019, San Diego, California. Reston, Virginia: AIAA, 2019.
- [71] Liu Q L, Baccarella D, Landsberg W, et al. Cavity flameholding in an optical axisymmetric scramjet in Mach 4.5 flows[J]. Proceedings of the Combustion Institute, 2019, 37(3): 3733-3740.
- [72] Tian Y, Zeng X J, Yang S H, et al. Experimental study on the effect of equivalence ratio and injector position on flow structure and flame development in the scramjet combustor[J]. Aerospace Science and Technology, 2018, 82/83: 9-19.
- [73] Halls B R, Gord J R, Meyer T R, et al. 20 kHz-rate three-dimensional tomographic imaging of the concentration field in a turbulent jet[J]. Proceedings of the Combustion Institute, 2017, 36(3): 4611-4618.
- [74] Wu Y, Xu W J, Ma L. Kilohertz VLIF (volumetric laser induced fluorescence) measurements in a seeded free gas-phase jet in the transitionally turbulent flow regime[J]. Optics and Lasers in Engineering, 2018, 102: 52-58.
- [75] Micka D, Driscoll J. Reaction zone imaging in a dual-mode scramjet combustor using CH-PLIF[C]//44th AIAA/ASME/SAE/ASEE Joint Propulsion Conference & Exhibit, July 21-23, 2008, Hartford, CT. Reston, Virginia: AIAA, 2008.
- [76] Micka D J, Driscoll J F. Stratified jet flames in a heated (1390 K) air cross-flow with autoignition[J]. Combustion and Flame, 2012, 159(3): 1205-1214.
- [77] Liang J H, Li Y, Sun M B, et al. CH-PLIF imaging of flame heat-release structures in supersonic combustion[J]. Journal of National University of Defense Technology, 2019, 41(1): 27-33.
梁剑寒, 李韵, 孙明波, 等. 超声速燃烧火焰放热区结构 CH-PLIF 成像技术[J]. 国防科技大学学报, 2019, 41(1): 27-33.
- [78] Rasmussen C C, Dhanuka S K, Driscoll J F. Visualization of flameholding mechanisms in a supersonic combustor using PLIF[J]. Proceedings of the Combustion Institute, 2007, 31(2): 2505-2512.
- [79] Allison P, Frederickson K, Kirik J W, et al. Investigation of flame structure and combustion dynamics using CH₂O PLIF and high-speed CH^{*} chemiluminescence in a premixed dual-mode scramjet combustor [C] // 54th AIAA Aerospace Sciences Meeting, January 4-8, 2016, San Diego, California, USA. Reston, Virginia: AIAA, 2016.
- [80] Gabet K N, Sutton J A. Narrowband versus broadband excitation for CH₂O PLIF imaging in flames using a frequency-tripled Nd : YAG laser[J]. Experiments in Fluids, 2014, 55(7): 1-11.
- [81] Paul P H, Najm H N. Planar laser-induced fluorescence imaging of flame heat release rate[J]. Symposium (International) on Combustion, 1998, 27(1): 43-50.
- [82] Wang J H, Zhang M, Huang Z H, et al. Measurement of the instantaneous flame front structure of syngas turbulent premixed flames at high pressure [J]. Combustion and Flame, 2013, 160(11): 2434-2441.
- [83] Zhang W J, Wang J H, Lin W J, et al. Effect of differential diffusion on turbulent lean premixed hydrogen enriched flames through structure analysis [J]. International Journal of Hydrogen Energy, 2020, 45(18): 10920-10931.
- [84] Zhang M, Wang J H, Xie Y L, et al. Measurement on instantaneous flame front structure of turbulent premixed CH₄/H₂/air flames [J]. Experimental Thermal and Fluid Science, 2014, 52: 288-296.
- [85] Wu Y, Modica V, Yu X L, et al. Effects of optical diagnostic techniques on the accuracy of laminar flame speeds measured from Bunsen flames: OH⁺ chemiluminescence, OH-PLIF and acetone/kerosene-PLIF [J]. Measurement Science and Technology, 2018, 29(1): 015204.
- [86] Skiba A W, Wabel T M, Carter C D, et al. Premixed flames subjected to extreme levels of turbulence part I: flame structure and a new measured regime diagram [J]. Combustion and Flame, 2018, 189: 407-432.
- [87] Bogdanoff D W. Advanced injection and mixing techniques for scramjet combustors [J]. Journal of Propulsion and Power, 1994, 10(2): 183-190.
- [88] Liu J, Gen H, Zhai Z, et al. Experimental investigation of transverse Jet in supersonic crossflow by acetone planar laser induced fluorescence[C]//1st Modern Aerodynamics & Aerothermodynamics Conference: Proceedings of 1st Modern Aerodynamics & Aerothermodynamics Conference. Shanghai: Chinese Society of Aerodynamics, 2006: 582-587.
刘君, 耿辉, 翟振辰, 等. 平面激光诱导荧光技术及其在横向喷流研究中的应用[C]//中国第一届近代空气动力学与气动热力学会议: 中国第一届近代空气动力学与气动热力学会议论文集. 上海: 中国空气动力学学会, 2006: 582-587.

- [89] Zhou M. Research on measurements of air mixing ratio using acetone planar laser induced fluorescence [D]. Harbin: Harbin Institute of Technology, 2015. 周森. 基于丙酮平面激光诱导荧光气流混合比测量研究[D]. 哈尔滨: 哈尔滨工业大学, 2015.
- [90] Severin M, Lammel O, Ax H, et al. High momentum jet flames at elevated pressure: detailed investigation of flame stabilization with simultaneous particle image velocimetry and OH-LIF[J]. *Journal of Engineering for Gas Turbines and Power*, 2018, 140(4): 041508.
- [91] Hartwig J, Mittal G, Sung C J. Acetone tracer laser-induced fluorescence (LIF) at 282 nm excitation as a diagnostic tool in elevated pressure and temperature systems[J]. *Applied Spectroscopy*, 2019, 73(4): 395-402.
- [92] Jenkins T P, Hess C F, Allison S W, et al. Measurements of turbine blade temperature in an operating aero engine using thermographic phosphors [J]. *Measurement Science and Technology*, 2020, 31(4): 044003.
- [93] Wang M R, Xiao Y, Han B, et al. Temperature field test for aeroengine combustor with five nozzles based on gas analysis [J]. *Journal of Aerospace Power*, 2016, 31(9): 2049-2054. 王明瑞, 肖阳, 韩冰, 等. 燃气分析法测量航空发动机五头部燃烧室温度场 [J]. *航空动力学报*, 2016, 31(9): 2049-2054.
- [94] Ezenwajiaku C, Talibi M, Doan N A K, et al. Study of polycyclic aromatic hydrocarbons (PAHs) in hydrogen-enriched methane diffusion flames [J]. *International Journal of Hydrogen Energy*, 2019, 44(14): 7642-7655.
- [95] Johchi A, Pareja J, Böhm B, et al. Quantitative mixture fraction imaging of a synthetic biogas turbulent jet propagating into a NO-vitiated air co-flow using planar laser-induced fluorescence (PLIF) [J]. *Experiments in Fluids*, 2019, 60(5): 1-13.
- [96] Lozano A, Yip B, Hanson R K. Acetone: a tracer for concentration measurements in gaseous flows by planar laser-induced fluorescence [J]. *Experiments in Fluids*, 1992, 13(6): 369-376.
- [97] Thurber M C, Grisch F, Kirby B J, et al. Measurements and modeling of acetone laser-induced fluorescence with implications for temperature-imaging diagnostics [J]. *Applied Optics*, 1998, 37(21): 4963-4978.
- [98] Thurber M C, Hanson R K. Pressure and composition dependences of acetone laser-induced fluorescence with excitation at 248, 266, and 308 nm [J]. *Applied Physics B*, 1999, 69(3): 229-240.
- [99] Rothamer D A, Snyder J A, Hanson R K, et al. Optimization of a tracer-based PLIF diagnostic for simultaneous imaging of EGR and temperature in IC engines [J]. *Applied Physics B*, 2010, 99(1/2): 371-384.
- [100] Miller V, Gamba M, Mungal G, et al. Toluene PLIF thermometry in supersonic flows [C] // 42nd AIAA Fluid Dynamics Conference and Exhibit, June 25-28, 2012, New Orleans, Louisiana. Reston, Virginia: AIAA, 2012.
- [101] Schulz C, Sick V. Tracer-LIF diagnostics: quantitative measurement of fuel concentration, temperature and fuel/air ratio in practical combustion systems [J]. *Progress in Energy and Combustion Science*, 2005, 31(1): 75-121.
- [102] Devillers R, Bruneaux G, Schulz C. Investigation of toluene LIF at high pressure and high temperature in an optical engine [J]. *Applied Physics B*, 2009, 96(4): 735-739.
- [103] Faust S, Tea G, Dreier T, et al. Temperature, pressure, and bath gas composition dependence of fluorescence spectra and fluorescence lifetimes of toluene and naphthalene [J]. *Applied Physics B*, 2013, 110(1): 81-93.
- [104] Thering H, Beckmann L, Jördens C, et al. Formaldehyde laser-induced fluorescence imaging with a multi-band transmission filter [J]. *Optics Letters*, 2014, 39(7): 1873-1876.
- [105] Kashitani M, Yamaguchi Y, Handa T, et al. Study on laser-induced acetone fluorescence in low-temperature gases of nitrogen and air [C] // 50th AIAA Aerospace Sciences Meeting including the New Horizons Forum and Aerospace Exposition, January 9-12, 2012, Nashville, Tennessee. Reston, Virginia: AIAA, 2012.
- [106] Sun M B, Geng H, Liang J H, et al. Mixing characteristics of gaseous fuel injection upstream of a flameholding cavity in supersonic flow [J]. *Journal of Propulsion Technology*, 2008, 29(3): 306-311. 孙明波, 耿辉, 梁剑寒, 等. 超声速来流稳焰凹腔上游气体燃料横向喷注的流动混合特征 [J]. *推进技术*, 2008, 29(3): 306-311.
- [107] Sun M B, Geng H, Liang J H, et al. Mixing characteristics in a supersonic combustor with gaseous fuel injection upstream of a cavity flameholder [J]. *Flow, Turbulence and Combustion*, 2009, 82(2): 271-286.
- [108] Yang L C, Peng J B, Li X H, et al. Planar laser-induced fluorescence imaging of kerosene injection in supersonic flow [J]. *Journal of Visualization*, 2019, 22(4): 751-760.

- [109] Etheridge S, Lee J G, Carter C, et al. Effect of flow distortion on fuel/air mixing and combustion in an upstream-fueled cavity flameholder for a supersonic combustor [J]. *Experimental Thermal and Fluid Science*, 2017, 88: 461-471.
- [110] Cantu L M L. Visualization and analysis of a hydrocarbon premixed flame a in small scale scramjet combustor[D]. Washington: The George Washington University, 2016.
- [111] Chun J. Experimental investigations of injection, mixing, and reaction processes in supersonic flow applications[D]. Stuttgart, Germany: University of Stuttgart, 2009.
- [112] Shi H, Tang Q L, An Y Z, et al. Study of spray/wall interaction in transition zones from HCCI via PPC to CI combustion modes[J]. *Fuel*, 2020, 268: 117341.
- [113] Salazar V M, Kaiser S A, Halter F. Optimizing precision and accuracy of quantitative PLIF of acetone as a tracer for hydrogen fuel[J]. *SAE International Journal of Fuels and Lubricants*, 2009, 2(1): 737-761.
- [114] Ji Y B, Yuan Y W, Ge B, et al. Study of the mixing and dilution characteristics of a RQL (rich-quench-lean) combustor in its quenching zone in an aeroengine[J]. *Journal of Engineering for Thermal Energy and Power*, 2016, 31(1): 48-53, 131-132.
吉雍彬, 袁用文, 葛冰, 等. 航空发动机 RQL 燃烧室淬熄区掺混特性研究[J]. *热能动力工程*, 2016, 31(1): 48-53, 131-132.
- [115] Yu Y. Experimental study and numerical simulation of gas flameless combustion induced by the inner structure [D]. Hefei: University of Science and Technology of China, 2010.
俞瑜. 气体引射式无焰燃烧的数值模拟和实验研究[D]. 合肥: 中国科学技术大学, 2010.
- [116] Dec J E, Canaan R E. PLIF imaging of NO formation in a DI diesel engine [EB/OL]. [2020-06-15]. [https:// www. researchgate. net/publication/300690588_PLIF_Imaging_of_NO_Formation_in_a_DI_Diesel_Engine](https://www.researchgate.net/publication/300690588_PLIF_Imaging_of_NO_Formation_in_a_DI_Diesel_Engine).
- [117] Mulla I A, Godard G, Cabot G, et al. Quantitative imaging of nitric oxide concentration in a turbulent n-heptane spray flame [J]. *Combustion and Flame*, 2019, 203: 217-229.
- [118] Williams B, Ewart P, Wang X W, et al. Quantitative planar laser-induced fluorescence imaging of multi-component fuel/air mixing in a firing gasoline-direct-injection engine: effects of residual exhaust gas on quantitative PLIF [J]. *Combustion and Flame*, 2010, 157(10): 1866-1878.
- [119] Marrero-Santiago J, Verdier A, Brunet C, et al. Experimental study of aeronautical ignition in a swirled confined jet-spray burner [J]. *Journal of Engineering for Gas Turbines and Power*, 2018, 140(2): 021502.
- [120] Lind S, Trost J, Zigan L, et al. Application of the tracer combination TEA/acetone for multi-parameter laser-induced fluorescence measurements in IC engines with exhaust gas recirculation [J]. *Proceedings of the Combustion Institute*, 2015, 35(3): 3783-3791.
- [121] Boggavarapu P, Ravikrishna R V. Quantitative vapour concentration measurements in n-dodecane and n-hexadecane sprays[J]. *Experimental Thermal and Fluid Science*, 2019, 102: 397-405.
- [122] Zhao W. Visualization research on gas injection characteristics of engine based on PLIF[D]. Harbin: Harbin Engineering University, 2018.
赵纬. 基于 PLIF 技术的天然气发动机燃气喷射特性研究[D]. 哈尔滨: 哈尔滨工程大学, 2018.
- [123] Ma X, He X, Qi Y L, et al. In-cylinder mixture distribution of direct injection LPG using laser-induced fluorescence [J]. *Transactions of CSICE*, 2009, 27(6): 481-486.
马骁, 何旭, 齐运亮, 等. 用激光诱导荧光法研究缸内直喷 LPG 混合气分布[J]. *内燃机学报*, 2009, 27(6): 481-486.
- [124] Ma X, He X, Wang J X, et al. In-cylinder mixture distribution measurement in a GDI engine using laser-induced fluorescence[J]. *Chinese Internal Combustion Engine Engineering*, 2010, 31(4): 1-5, 10.
马骁, 何旭, 王建昕, 等. 用激光诱导荧光法测量 GDI 发动机缸内混合气分布[J]. *内燃机工程*, 2010, 31(4): 1-5, 10.
- [125] Miller V A, Gamba M, Mungal M G, et al. Single- and dual-band collection toluene PLIF thermometry in supersonic flows [J]. *Experiments in Fluids*, 2013, 54(6): 1-13.
- [126] Gamba M, Miller V A, Mungal M G, et al. Temperature and number density measurement in non-uniform supersonic flowfields undergoing mixing using toluene PLIF thermometry[J]. *Applied Physics B*, 2015, 120(2): 285-304.
- [127] Snyder J A. Development and application of tracer-based planar laser-induced fluorescence imaging diagnostics for HCCI engines [D]. Stanford, California, USA: Stanford University, 2011.
- [128] Willman C, Stone R, Davy M, et al. Cycle-to-cycle variation analysis of two-colour PLIF temperature measurements calibrated with laser induced grating

- spectroscopy in a firing GDI engine [J]. SAE International Journal of Advances and Current Practices in Mobility, 2019, 1(4): 1404-1419.
- [129] Dronniou N, Dec J E. Investigating the development of thermal stratification from the near-wall regions to the bulk-gas in an HCCI engine with planar imaging thermometry [J]. SAE International Journal of Engines, 2012, 5(3): 1046-1074.
- [130] Zhang W L, Fu X Q, He B Q. PLIF-based temperature and concentration measurement of in-cylinder mixture and its application [J]. Journal of Safety Science and Technology, 2014, 10(9): 61-66. 张万里, 付雪青, 何邦全. 基于 PLIF 的混合气温度和浓度测量及其应用 [J]. 中国安全生产科学技术, 2014, 10(9): 61-66.
- [131] Yan B, Chen L, Chen S, et al. Structured illumination for two-dimensional laser induced fluorescence imaging to eliminate stray light interference [J]. Acta Physica Sinica, 2019, 68(21): 218701. 闫博, 陈力, 陈爽, 等. 结构光照明技术在二维激光诱导荧光成像去杂散光中的应用 [J]. 物理学报, 2019, 68(21): 218701.
- [132] Yan B, Su T, Chen S, et al. Structured illumination for Rayleigh scattering imaging to eliminate the stray light interference [J]. Journal of Experiments in Fluid Mechanics, 2020, 34(1): 33-37, 48. 闫博, 苏轶, 陈爽, 等. 结构光照明技术在瑞利散射成像去杂散光应用中的研究 [J]. 实验流体力学, 2020, 34(1): 33-37, 48.
- [133] Yan B, Chen L, Li M, et al. Quantitative temperature imaging at elevated pressures and in a confined space with CH₄/air laminar flames by filtered Rayleigh scattering [J]. Chinese Physics B, 2020, 29(2): 024701.
- [134] Saiki Y, Kurimoto N, Suzuki Y, et al. Active control of jet premixed flames in a model combustor with manipulation of large-scale vortical structures and mixing [J]. Combustion and Flame, 2011, 158(7): 1391-1403.
- [135] Joklik R G, Daily J W. Two-line atomic fluorescence temperature measurement in flames: an experimental study [J]. Applied Optics, 1982, 21(22): 4158-4162.
- [136] Daily J W. Laser induced fluorescence spectroscopy in flames [J]. Progress in Energy and Combustion Science, 1997, 23(2): 133-199.
- [137] Fang B L, Hu Z Y, Zhang Z R, et al. Mechanism of laser induced fluorescence signal generation in InCl₃-ethanol mixture flames [J]. Proceedings of SPIE, 2017, 1017: 1017312.
- [138] Chan Q N, Medwell P R, Kalt P A M, et al. Simultaneous imaging of temperature and soot volume fraction [J]. Proceedings of the Combustion Institute, 2011, 33(1): 791-798.
- [139] Chan Q N, Medwell P R, Dally B B, et al. New seeding methodology for gas concentration measurements [J]. Applied Spectroscopy, 2012, 66(7): 803-809.
- [140] Münsterjohann B, Huber F J T, Klima T C, et al. Potential of two-line atomic fluorescence for temperature imaging in turbulent indium-oxide-producing flames [J]. Journal of Nanoparticle Research, 2015, 17(11): 1-10.
- [141] Whiddon R, Zhou B, Borggren J, et al. Vapor phase tri-methyl-indium seeding system suitable for high temperature spectroscopy and thermometry [J]. The Review of Scientific Instruments, 2015, 86(9): 093107.
- [142] Dec J E, Keller J O. High speed thermometry using two-line atomic fluorescence [J]. Symposium (International) on Combustion, 1988, 21(1): 1737-1745.
- [143] Burns I S, Mercier X, Wartel M, et al. A method for performing high accuracy temperature measurements in low-pressure sooting flames using two-line atomic fluorescence [J]. Proceedings of the Combustion Institute, 2011, 33(1): 799-806.
- [144] Löfström C, Engström J, Richter M, et al. Feasibility studies and application of laser /optical diagnostics for characterisation of a practical low-emission gas turbine combustor [C] // Proceedings of ASME Turbo Expo 2000: Power for Land, Sea, and Air, May 8-11, 2000, Munich, Germany. New York: ASME, 2000: 1-8.
- [145] Medwell P R, Chan Q N, Kalt P A, et al. Instantaneous temperature imaging of diffusion flames using two-line atomic fluorescence [J]. Applied Spectroscopy, 2010, 64(2): 173-176.
- [146] Chan Q N, Medwell P R, Alwahabi Z T, et al. Assessment of interferences to nonlinear two-line atomic fluorescence (NTLAF) in sooty flames [J]. Applied Physics B, 2011, 104(1): 189-198.
- [147] Gu D H, Sun Z W, Nathan G J, et al. Improvement of precision and accuracy of temperature imaging in sooting flames using two-line atomic fluorescence (TLAF) [J]. Combustion and Flame, 2016, 167: 481-493.
- [148] Manteghi A A. Probing gases and flames by coherent rayleigh brillouin scattering and two lines atomic fluorescence [D]. Eindhoven, Netherlands: Eindhoven University of Technology, 2013.

- [149] Foo K K, Sun Z W, Medwell P R, et al. Experimental investigation of acoustic forcing on temperature, soot volume fraction and primary particle diameter in non-premixed laminar flames[J]. *Combustion and Flame*, 2017, 181: 270-282.
- [150] Sun Z W, Alwahabi Z, Dally B, et al. Simultaneously calibrated two-line atomic fluorescence for high-precision temperature imaging in sooting flames[J]. *Proceedings of the Combustion Institute*, 2019, 37(2): 1417-1425.
- [151] Fang B L, Hu Z Y, Tao B, et al. New calibration method for nonlinear two-line atomic fluorescence [J]. *Acta Optica Sinica*, 2017, 37(11): 1112001.
方波浪, 胡志云, 陶波, 等. 非线性双线原子荧光技术的标定新方法 [J]. *光学学报*, 2017, 37(11): 1112001.
- [152] Fang B L, Zhang Z R, Li G H, et al. Simple calibrated nonlinear excitation regime two-line atomic fluorescence thermometry[J]. *Optics Letters*, 2019, 44(2): 227-230.
- [153] Sijtsema N M, Dam N J, Klein-Douwel R J H, et al. Air photolysis and recombination tracking: a new molecular tagging velocimetry scheme [J]. *AIAA Journal*, 2002, 40(6): 1061-1064.
- [154] Bearden W C, Hall C A, Pitz R W. Examination of NO tag formation for unseeded molecular tagging velocimetry [C] // 55th AIAA Aerospace Sciences Meeting, January 9-13, 2017, Grapevine, Texas. Reston, Virginia: AIAA, 2017.
- [155] ElBaz A M, Pitz R W. N₂O molecular tagging velocimetry[J]. *Applied Physics B*, 2012, 106(4): 961-969.
- [156] Orlemann C, Schulz C, Wolfrum J. NO-flow tagging by photodissociation of NO₂. A new approach for measuring small-scale flow structures[J]. *Chemical Physics Letters*, 1999, 307(1/2): 15-20.
- [157] Bathel B, Danehy P, Jones S, et al. Trip-induced transition measurements in a hypersonic boundary layer using molecular tagging velocimetry [C] // 51st AIAA Aerospace Sciences Meeting including the New Horizons Forum and Aerospace Exposition, January 7-10, 2013, Grapevine (Dallas/Ft. Worth Region), Texas. Reston, Virginia: AIAA, 2013.
- [158] Parziale N J, Smith M S, Marineau E C. Krypton tagging velocimetry of an underexpanded jet [J]. *Applied Optics*, 2015, 54(16): 5094-5101.
- [159] Mustafa M A, Parziale N J, Smith M S, et al. Nonintrusive freestream velocity measurement in a large-scale hypersonic wind tunnel [J]. *AIAA Journal*, 2017, 55(10): 3611-3616.
- [160] Pitz R W, Wehrmeyer J A, Ribarov L A, et al. Unseeded molecular flow tagging in cold and hot flows using ozone and hydroxyl tagging velocimetry [J]. *Measurement Science and Technology*, 2000, 11(9): 1259-1271.
- [161] Ribarov L A, Hu S T, Wehrmeyer J A, et al. Hydroxyl tagging velocimetry method optimization: signal intensity and spectroscopy[J]. *Applied Optics*, 2005, 44(31): 6616-6626.
- [162] Hall C A, Ramsey M C, Knaus D A, et al. Molecular tagging velocimetry in nitrogen with trace water vapor[J]. *Measurement Science and Technology*, 2017, 28(8): 085201.
- [163] Dam N, Klein-Douwel R J, Sijtsema N M, et al. Nitric oxide flow tagging in unseeded air[J]. *Optics Letters*, 2001, 26(1): 36-38.
- [164] Laan W P N, Tolboom R A L, Dam N J, et al. Molecular tagging velocimetry in the wake of an object in supersonic flow[J]. *Experiments in Fluids*, 2003, 34(4): 531-534.
- [165] Bathel B, Johansen C, Danehy P, et al. Hypersonic boundary layer transition measurements using NO₂⁻>NO photo-dissociation tagging velocimetry [C] // 41st AIAA Fluid Dynamics Conference and Exhibit, June 27-30, 2011, Honolulu, Hawaii. Reston, Virginia: AIAA, 2011.
- [166] Bathel B, Danehy P, Johansen C, et al. Hypersonic boundary layer measurements with variable blowing rates using molecular tagging velocimetry [C] // 28th Aerodynamic Measurement Technology, Ground Testing, and Flight Testing Conference, June 25-28, 2012, New Orleans, Louisiana Reston, Virginia: AIAA, 2012.
- [167] Kidd F G, Narayanaswamy V, Danehy P M, et al. Characterization of the NASA langley arc heated scramjet test facility using NO PLIF [C] // 30th AIAA Aerodynamic Measurement Technology and Ground Testing Conference, June 16-20, 2014, Atlanta, GA. Reston, Virginia: AIAA, 2014.
- [168] Sánchez-González R, Bowersox R D W, North S W. Simultaneous velocity and temperature measurements in gaseous flowfields using the vibrationally excited nitric oxide monitoring technique: a comprehensive study[J]. *Applied Optics*, 2012, 51(9): 1216-1228.
- [169] Sánchez-González R, Bowersox R D, North S W. Vibrationally excited NO tagging by NO(A²Σ⁺) fluorescence and quenching for simultaneous velocimetry and thermometry in gaseous flows [J]. *Optics Letters*, 2014, 39(9): 2771-2774.
- [170] Dai S T, Jiang T, Wu H C, et al. Tunable narrowlinewidth 226 nm laser for hypersonic flow velocimetry[J]. *Optics Letters*, 2020, 45(8): 2291-

- 2294.
- [171] Parziale N J, Smith M, Marineau E C. Krypton tagging velocimetry for use in high-speed ground-test facilities [C] // 53rd AIAA Aerospace Sciences Meeting, January 5-9, 2015, Kissimmee, Florida. Reston, Virginia: AIAA, 2015.
- [172] Zahradka D, Parziale N J, Smith M S, et al. Krypton tagging velocimetry in a turbulent Mach 2.7 boundary layer[J]. *Experiments in Fluids*, 2016, 57(5): 1-14.
- [173] Mustafa M A, Parziale N J. Simplified read schemes for krypton tagging velocimetry in N_2 and air [J]. *Optics Letters*, 2018, 43(12): 2909-2912.
- [174] Mustafa M A, Parziale N J, Marineau E C, et al. Two-dimensional krypton tagging velocimetry (KTV-2D) investigation of shock-wave/turbulent boundary-layer interaction[C]//2018 AIAA Aerospace Sciences Meeting, January 8-12, 2018, Kissimmee, Florida. Reston, Virginia: AIAA, 2018.
- [175] Mustafa M A, Parziale N J, Smith M S, et al. Amplification and structure of streamwise-velocity fluctuations in compression-corner shock-wave/turbulent boundary-layer interactions [J]. *Journal of Fluid Mechanics*, 2019, 863: 1091-1122.
- [176] Mustafa M A, Shekhtman D, Parziale N J. Single-laser krypton tagging velocimetry (KTV) investigation of air and N_2 boundary-layer flows over a hollow cylinder in the Stevens shock tube [C] // AIAA Scitech 2019 Forum, January 7-11, 2019, San Diego, California. Reston, Virginia: AIAA, 2019.
- [177] Ribarov L A, Wehrmeyer J A, Pitz R W, et al. Hydroxyl tagging velocimetry (HTV) in experimental air flows[J]. *Applied Physics B*, 2002, 74(2): 175-183.
- [178] Grady N, Pitz R W. Vibrationally excited hydroxyl tagging velocimetry [J]. *Applied Optics*, 2014, 53(31): 7182-7188.
- [179] Ramsey M C, Pitz R W, Jenkins T P, et al. Planar 2D velocity measurements in the cap shock pattern of a thrust optimized rocket nozzle [J]. *Shock Waves*, 2012, 22(1): 39-46.
- [180] Lahr M D, Pitz R W, Douglas Z W, et al. Hydroxyl-tagging-velocimetry measurements of a supersonic flow over a cavity [J]. *Journal of Propulsion and Power*, 2010, 26(4): 790-797.
- [181] Grady N R, Pitz R W, Carter C D, et al. Supersonic flow over a ramped-wall cavity flame holder with an upstream strut[J]. *Journal of Propulsion and Power*, 2012, 28(5): 982-990.
- [182] Pitz R, Lahr M, Douglas Z, et al. Hydroxyl tagging velocimetry in a Mach 2 flow with a wall cavity[C]// 43rd AIAA Aerospace Sciences Meeting and Exhibit, January 10-13, 2005, Reno, Nevada. Reston, Virginia: AIAA, 2005.
- [183] Ramsey M C, Pitz R W. Template matching for improved accuracy in molecular tagging velocimetry [J]. *Experiments in Fluids*, 2011, 51(3): 811-819.
- [184] Shao J, Ye J F, Hu Z Y, et al. Method to improve signal extraction capability of hydroxyl tagging velocimetry in supersonic combustion flow field [J]. *Acta Photonica Sinica*, 2019, 48(9): 0912007. 邵珺, 叶景峰, 胡志云, 等. 一种提高超燃流场羟基示踪速度测量中信号提取能力的方法 [J]. *光子学报*, 2019, 48(9): 0912007.
- [185] Shao J, Fang B L, Ye J F, et al. Method to improve the velocimetry measurement accuracy of hydroxyl tagging velocimetry in complex combustion flow field [J]. *Acta Photonica Sinica*, 2019, 48(4): 0412001. 邵珺, 方波浪, 叶景峰, 等. 提高复杂燃烧流场羟基示踪测速精度的方法 [J]. *光子学报*, 2019, 48(4): 0412001.
- [186] Shao J, Ye J F, Wang S, et al. Background noise suppress method for hydroxyl tagging velocimetry in combustion flow field [J]. *Chinese Journal of Lasers*, 2019, 46(3): 0309001. 邵珺, 叶景峰, 王晟, 等. 燃烧流场羟基示踪测速的噪声去除方法 [J]. *中国激光*, 2019, 46(3): 0309001.
- [187] Hu Z Y, Ye J F, Zhang Z R, et al. Development of laser combustion diagnostic techniques for ground aero-engine testing [J]. *Journal of Experiments in Fluid Mechanics*, 2018, 32(1): 33-42. 胡志云, 叶景峰, 张振荣, 等. 航空发动机地面试验激光燃烧诊断技术研究进展 [J]. *实验流体力学*, 2018, 32(1): 33-42.
- [188] Pan F, Sánchez-González R, McIlvoy M H, et al. Simultaneous three-dimensional velocimetry and thermometry in gaseous flows using the stereoscopic vibrationally excited nitric oxide monitoring technique [J]. *Optics Letters*, 2016, 41(7): 1376-1379.
- [189] Hammack S D, Lee T, Hsu K Y, et al. High-repetition-rate OH planar laser-induced fluorescence of a cavity flameholder [J]. *Journal of Propulsion and Power*, 2013, 29(5): 1248-1251.
- [190] Jiang N B, Webster M C, Lempert W R. Advances in generation of high-repetition-rate burst mode laser output [J]. *Applied Optics*, 2009, 48(4): B23-B31.
- [191] Peng J B, Cao Z, Yu X, et al. Continuous 500-Hz OH-PLIF measurements in a hydrogen-fueled scramjet combustor [J]. *Frontiers in Physics*, 2020, 8: 101.
- [192] Yang X Y, Fu C, Wang G Q, et al. Simultaneous

- high-speed SO_2 PLIF imaging and stereo-PIV measurements in premixed swirling flame at 20 kHz [J]. *Applied Optics*, 2019, 58(10): C121-C129.
- [193] Wang S R, Liu X C, Wang G Q, et al. High-repetition-rate burst-mode-laser diagnostics of an unconfined lean premixed swirling flame under external acoustic excitation [J]. *Applied Optics*, 2019, 58(10): C68-C78.
- [194] Wellander R, Richter M, Aldén M. Time-resolved (kHz) 3D imaging of OH PLIF in a flame [J]. *Experiments in Fluids*, 2014, 55(6): 1-12.
- [195] Xu W J, Carter C D, Hammack S, et al. Analysis of 3D combustion measurements using CH-based tomographic VLIF (volumetric laser induced fluorescence) [J]. *Combustion and Flame*, 2017, 182: 179-189.
- [196] Halls B R, Hsu P S, Ethan L, et al. 3D OH LIF measurements in a lifted flame [C] // 55th AIAA Aerospace Sciences Meeting, January 9-13, 2017, Grapevine, Texas. Reston, Virginia: AIAA, 2017.
- [197] Liu N, Ma L. 3D flame measurements using tomography reconstruction integrating view registration [C] // AIAA Scitech 2020 Forum, January 6-10, 2020, Orlando, FL, USA. Reston, Virginia: AIAA, 2020.
- [198] Ma L, Lei Q C, Wu Y, et al. From ignition to stable combustion in a cavity flameholder studied via 3D tomographic chemiluminescence at 20 kHz [J]. *Combustion and Flame*, 2016, 165: 1-10.
- [199] Shimura M, Ueda T, Choi G M, et al. Simultaneous dual-plane CH PLIF, single-plane OH PLIF and dual-plane stereoscopic PIV measurements in methane-air turbulent premixed flames [J]. *Proceedings of the Combustion Institute*, 2011, 33(1): 775-782.
- [200] Boxx I, Slabaugh C, Kutne P, et al. 3 kHz PIV/OH-PLIF measurements in a gas turbine combustor at elevated pressure [J]. *Proceedings of the Combustion Institute*, 2015, 35(3): 3793-3802.
- [201] Fuest F, Barlow R S, Chen J Y, et al. Raman/Rayleigh scattering and CO-LIF measurements in laminar and turbulent jet flames of dimethyl ether [J]. *Combustion and Flame*, 2012, 159(8): 2533-2562.
- [202] Jeong C, Bae J, Kim T, et al. Investigation of flashback characteristics coupled with combustion instability in turbulent premixed bluff body flames using high-speed OH-PLIF and PIV [J]. *Proceedings of the Combustion Institute*, 2017, 36(2): 1861-1868.
- [203] Fugger C A, Roy S, Caswell A W, et al. Structure and dynamics of CH_2O , OH, and the velocity field of a confined bluff-body premixed flame, using simultaneous PLIF and PIV at 10 kHz [J]. *Proceedings of the Combustion Institute*, 2019, 37(2): 1461-1469.
- [204] Skiba A W, Carter C D, Hammack S D, et al. The influence of large eddies on the structure of turbulent premixed flames characterized with stereo-PIV and multi-species PLIF at 20 kHz [J]. *Proceedings of the Combustion Institute*, 2019, 37(2): 2477-2484.
- [205] Weinkauff J, Trunk P, Frank J H, et al. Investigation of flame propagation in a partially premixed jet by high-speed-stereo-PIV and acetone-PLIF [J]. *Proceedings of the Combustion Institute*, 2015, 35(3): 3773-3781.
- [206] Hammack S D, Skiba A W, Lee T, et al. CH PLIF and PIV implementation using C-X (0, 0) and intravibrational band filtered detection [J]. *Applied Physics B*, 2018, 124(2): 1-5.
- [207] Mitsingas C M, Hammack S D, Mayhew E K, et al. Simultaneous high speed PIV and CH PLIF using R-branch excitation in the $\text{C}^2\Sigma^+ - \text{X}^2\Pi$ (0, 0) band [J]. *Proceedings of the Combustion Institute*, 2019, 37(2): 1479-1487.
- [208] Gao Y, Yang X Y, Fu C, et al. 10 kHz simultaneous PIV/PLIF study of the diffusion flame response to periodic acoustic forcing [J]. *Applied Optics*, 2019, 58(10): C112-C120.
- [209] Guo S L, Wang J H, Zhang W J, et al. Effect of hydrogen enrichment on swirl/bluff-body lean premixed flame stabilization [J]. *International Journal of Hydrogen Energy*, 2020, 45(18): 10906-10919.
- [210] Guo S L, Wang J H, Zhang W J, et al. Investigation on bluff-body and swirl stabilized flames near lean blowoff with PIV/PLIF measurements and LES modelling [J]. *Applied Thermal Engineering*, 2019, 160: 114021.
- [211] Fan X J, Liu C X, Xu G, et al. Experimental investigations of the spray structure and interactions between sectors of a double-swirl low-emission combustor [J]. *Chinese Journal of Aeronautics*, 2020, 33(2): 589-597.
- [212] Chtereve I, Rock N, Ek H, et al. Simultaneous imaging of fuel, OH, and three component velocity fields in high pressure, liquid fueled, swirl stabilized flames at 5 kHz [J]. *Combustion and Flame*, 2017, 186: 150-165.
- [213] Skiba A W, Carter C D, Hammack S D, et al. A simplified approach to simultaneous multi-scalar imaging in turbulent flames [J]. *Combustion and Flame*, 2018, 189: 207-211.

- [214] Kong C D, Li Z S, Aldén M, et al. Stabilization of a turbulent premixed flame by a plasma filament [J]. *Combustion and Flame*, 2019, 208: 79-85.
- [215] Novoselov A G, Reuter C B, Yehia O R, et al. Turbulent nonpremixed cool flames: experimental measurements, direct numerical simulation, and manifold-based combustion modeling [J]. *Combustion and Flame*, 2019, 209: 144-154.
- [216] Ge B, Ji Y B, Zhang Z L, et al. Experiment study on the combustion performance of hydrogen-enriched natural gas in a DLE burner [J]. *International Journal of Hydrogen Energy*, 2019, 44(26): 14023-14031.
- [217] Do H, Im S K, Cappelli M A, et al. Plasma assisted flame ignition of supersonic flows over a flat wall [J]. *Combustion and Flame*, 2010, 157(12): 2298-2305.
- [218] Jain A, Wang Y J, Kulatilaka W D. Effect of H-atom concentration on soot formation in premixed ethylene/air flames [J]. *Proceedings of the Combustion Institute*, 2019, 37(2): 1289-1296.
- [219] Guiberti T F, Boyette W R, Krishna Y, et al. Assessment of the stabilization mechanisms of turbulent lifted jet flames at elevated pressure using combined 2-D diagnostics [J]. *Combustion and Flame*, 2020, 214: 323-335.
- [220] Liu Y Z, He Y, Wang Z H, et al. Multi-point LIBS measurement and kinetics modeling of sodium release from a burning Zhundong coal particle [J]. *Combustion and Flame*, 2018, 189: 77-86.
- [221] Park O, Burns R A, Clemens N T. Relationship between soot and scalar dissipation rate in the soot-inception region of turbulent non-premixed jet flames [J]. *Proceedings of the Combustion Institute*, 2019, 37(1): 1057-1064.
- [222] Köser J, Li T, Vorobiev N, et al. Multi-parameter diagnostics for high-resolution in situ measurements of single coal particle combustion [J]. *Proceedings of the Combustion Institute*, 2019, 37(3): 2893-2900.
- [223] Balusamy S, Kamal M M, Lowe S M, et al. Laser diagnostics of pulverized coal combustion in O_2/N_2 and O_2/CO_2 conditions: velocity and scalar field measurements [J]. *Experiments in Fluids*, 2015, 56(5): 1-16.
- [224] Wang Y H, Song W Y, Shi D Y. Experimental study of flame stabilization in a kerosene fueled scramjet combustor [J]. *Acta Astronautica*, 2019, 157: 282-293.
- [225] Malbois P, Salaün E, Vandel A, et al. Experimental investigation of aerodynamics and structure of a swirl-stabilized kerosene spray flame with laser diagnostics [J]. *Combustion and Flame*, 2019, 205: 109-122.

Research Progress of Laser-Induced Fluorescence Technology in Combustion Diagnostics

Zhu Jiajian^{*}, Wan Minggang, Wu Ge, Yan Bo, Tian Yifu, Feng Rong, Sun Mingbo

Science and Technology on Scramjet Laboratory, College of Aerospace Science and Engineering, National University of Defense Technology, Changsha, Hunan 410073, China

Abstract

Significance Laser-induced fluorescence (LIF) can be used to perform non-intrusive, in-situ, and temporally and spatially resolved measurements of combustion characteristics with strong species selectivity and good sensitivity. This paper reviews research progress in the development and application of multi-species planar LIF (PLIF), tracer PLIF and PLIF-based velocimetry in combustion diagnostics to measure instantaneous flame structure, fuel concentration, temperature, and velocity. This work also discusses the typical examples, characteristics, and challenges of conducting PLIF in fundamental combustion diagnostics and practical engine measurements. The technological trends about high-repetition PLIF, volumetric LIF (VLIF), and simultaneous multi-parameter measurements are also presented.

Progress The PLIF can visualize the two-dimensional distributions of multi-species generated during the combustion process and show the instantaneous flame structure. The formaldehyde (CH_2O) can be used as an indicator of the flame preheating zone, and OH radicals can be regarded as a flame marker of the product zone. Simultaneous PLIF measurements of the CH_2O and OH can obtain the heat release zone of a premixed turbulent flame shown in **Fig. 6(a)**. **Fig. 6(b)** and **Fig. 6(c)** show CH_2O and OH PLIF images that are acquired simultaneously as well as the distributions of the heat release zone that are obtained by the pixel-by-pixel product of OH and CH_2O . CH

radicals in flames are usually employed to indicate the flame reaction zone. The CH radicals are difficult to be measured by PLIF due to their relatively low concentration in flames. The signal-to-noise ratio of the CH PLIF can be significantly improved by using a high-energy tunable Alexandrite laser at ~ 387 nm and the C-X excitation at ~ 314 nm. The distributed reaction zone can be identified in a high-speed jet flame by broadening CH distributions that can be observed by the CH-PLIF. The HCO and CH_3 radicals that indicate instantaneous flame structure can be measured by single-shot HCO PLIF and photofragmentation LIF, and the two-dimensional distributions of HCO and CH_3 are shown in **Fig. 6(c)** and **Fig. 6(d)**, respectively. The OH, CH, and CH_2O PLIF can be used to obtain instantaneous flame structures in a cavity-based scramjet combustor, which helps to better understand the flameholding modes and mechanism in a supersonic flow. Feature extraction of the turbulent flame front, the flame surface density, the progressive variable, and the ridge can be achieved from the PLIF images, which gives quantitative information of the flame structure and sheds light on interactions between combustion and turbulence.

The tracer PLIF can measure fuel concentration, equivalence ratio, and temperature during the mixing process by adding fluorescent tracers into small-scale burners or practical combustion systems. Characteristics of the frequently used tracer molecules are described, such as acetone, 3-Pentanone, toluene, and NO. Typical applications of the tracer PLIF in showing the fuel distribution, equivalence ratio, and temperature distribution during the mixing process of different engines are introduced. The two-line atomic fluorescence (TLAF) can be used to indicate the two-dimensional distribution of the flame temperature by seeding atomic elements into a flame. Temperature characteristics of typical atomic elements (e.g. gallium, indium, and thallium) are compared, and different seeding methods for the indium atom are introduced. Linear and nonlinear TLAF methods with the indium atom seeding can be used to show two-dimensional distributions of the flame temperature. Nonlinear TLAF is a promising technique for two-dimensional temperature measurements in a harsh environment with an acceptable signal-to-noise ratio. The challenges of conducting the tracer PLIF in quantitative measurements are presented. Accurate calibrations of the fluorescence intensity in different conditions of temperature and pressure play a key role in the quantitative measurements of the tracer PLIF and TLAF techniques.

The PLIF techniques can be used in molecular tagging velocimetry (MTV) to non-intrusively measure the velocity distribution of the flow field. In the MTV technique, a 'write' laser pulse is employed to generate flow tracer (e.g. NO, Kr and OH) with a relatively long-lifetime fluorescence through the process of photodissociation, excitation, or photochemical reaction, and then a 'read' laser pulse is used to tag the location displacement and the delay time of the tracers. The NO PLIF, Kr PLIF, and OH PLIF are usually adopted during the 'read' process of the MTV technique. The air photolysis and recombination tracking (APART)/vibrationally excited NO monitoring (VENOM), krypton tagging velocimetry (KTV), and hydroxyl tagging velocimetry (HTV) have been widely used in measuring the velocity distribution in a cold or reacting flow ranging from low to hypersonic velocity.

Conclusion and Prospect LIF is a non-intrusive and in-situ technique, which can be used to accurately measure instantaneous flame structure, fuel concentration, temperature, and velocity of flames and engine combustion. The repetition rate and measurement dimension of LIF techniques are required to be further improved. With the development of high-energy and high-repetition pulsed lasers, the high-speed PLIF technology (10 – 1000 kHz) can show the dynamic evolution of instantaneous flame structure during the process of flame ignition, flameout, and combustion oscillation. The VLIF technology can be employed to demonstrate the three-dimensional structure of the flame and realize four-dimensional (three-dimensional + t) measurements in combination with a high-speed laser. The PLIF can be synchronized with PIV, Rayleigh scattering, and other techniques to realize the simultaneous visualization of instantaneous flame structure, flow velocity, and flame temperature, which helps to further reveal the interaction mechanism of combustion and turbulence.

The applications of the PLIF techniques in practical engines need to solve many problems, such as complex optical path adjustment and optical window design, stray light suppression, and signal-to-noise ratio optimization. The combustion information obtained by the PLIF techniques is still limited. The PLIF techniques need to be combined with other measurement methods, theoretical models, and numerical simulations to better understand the characteristics and mechanisms of combustion.

Key words spectroscopy; laser-induced fluorescence; combustion diagnostics; engines; flame structure; temperature; flow velocity

OCIS codes 300.2530; 120.1740; 280.2470; 280.2490